2008

Ongoing assembly of massive galaxies by major merging in large groups and clusters from the SDSS

DH McIntosh

YC Guo

J Hertzberg

N Katz
University of Massachusetts - Amherst

HJ Mo

See next page for additional authors

DRAFT: February 2, 2008

Ongoing Assembly of Massive Galaxies by Major Merging in Large Groups and Clusters from the SDSS

Daniel H. McIntosh[1,2], Yicheng Guo[1], Jen Hertzberg[1,3], Neal Katz[1], H. J. Mo[1]

Frank C. van den Bosch[4], Xiaohu Yang[5,6]

[1] *Astronomy Department, University of Massachusetts, 710 N. Pleasant St., Amherst, MA 01003, USA*

[2] *email: dmac@hamerkop.astro.umass.edu*

[3] *Current address: Stony Brook University, Marine Sciences Research Center, Stony Brook, NY 11794-5000*

[4] *Max-Planck-Institut für Astronomie, Königstuhl 17, D-69117 Heidelberg, Germany*

[5] *Shanghai Astronomical Observatory, the Partner Group of MPA, Nandan Road 80, Shanghai 200030, China*

[6] *Joint Institute for Galaxy and Cosmology of Shanghai Astronomical Observatory and University of Science and Technology of China*

ABSTRACT

We investigate the incidence of major mergers creating $\mathrm{M_{star}} > 10^{11}\mathrm{M_\odot}$ galaxies in the dense environments of present-day groups and clusters more massive than $\mathrm{M_{halo}} = 2.5 \times 10^{13}\mathrm{M_\odot}$. We identify 38 pairs of massive galaxies with mutual tidal interaction signatures selected from > 5000 galaxies with $\mathrm{M_{star}} \geq 5{\times}10^{10}\mathrm{M_\odot}$ that reside in a halo mass-limited sample of 845 groups. We fit the images of each galaxy pair as the line-of-sight projection of symmetric models and identify mergers by the presence of residual asymmetric structure associated with both progenitors, such as nonconcentric isophotes, broad and diffuse tidal tails, and dynamical friction wakes. At the resolution and sensitivity of the SDSS, such mergers are found in 16% of the high-mass, galaxy-galaxy pairs with ≤ 1.5 r-band magnitude differences and ≤ 30 kpc projected separations. Relying on automated searches of major pairs from the SDSS spectroscopic galaxy sample will result in missing 70% of these mergers owing to spectroscopic incompleteness in high-density regions. We find that 90% of these mergers are between two nearly equal-mass progenitors with red-sequence colors and centrally-concentrated morphologies, in agreement with numerical simulations that predict that an important mechanism for the formation of massive elliptical galaxies is the dissipationless (gas-poor or so-called dry) major merging of spheroid-dominated galaxies. We identify seven additional $\mathrm{M_{star}} > 10^{11}\mathrm{M_\odot}$ mergers with disturbed morphologies and semi-resolved double nuclei. Mergers at the centers

of massive groups are more common than between two satellites, but both types are morphologically indistinguishable and we tentatively conclude that the latter are likely located at the dynamical centers of large subhalos that have recently been accreted by their host halo, rather than the centers of distinct halos seen in projection. We find that the frequency of central and satellite merging diminishes with group mass in a manner that is consistent with dynamical friction. Based on reasonable assumptions, the centers of these massive halos are gaining stellar mass at a rate of 1–9% per Gyr on average. Compared to the merger rate for the overall population of luminous red galaxies, we find that the rate is 2–9 times greater when restricted to these dense environments. Our results imply that the massive end of the galaxy population continues to evolve hierarchically at a measurable level, and that the centers of massive groups are the preferred environment for the merger-driven assembly of massive ellipticals.

Subject headings: galaxies: evolution — galaxies: fundamental parameters (luminosities, stellar masses, radii) — galaxies: general — surveys

1. Introduction

Understanding the formation of the most-massive galaxies ($\mathrm{M_{star}} > 10^{11}\mathrm{M_{\odot}}$) remains an important challenge in astrophysics. The tip of the stellar mass function is dominated by elliptical galaxies with intrinsically spheroidal mass distributions that are supported by anisotropic stellar motions (Kormendy & Bender 1996; Burstein et al. 1997). Numerical simulations have long demonstrated that "major" mergers between smaller galaxies of comparable mass could produce the observed shapes and dynamics of ellipticals (Toomre 1977; Barnes & Hernquist 1996; Naab & Burkert 2003; Cox et al. 2006). Moreover, massive ellipticals are found in greater abundance in high-density structures like large groups and clusters of galaxies (e.g., Dressler 1980; Postman & Geller 1984; Hashimoto & Oemler 1999; Smith et al. 2005), which naturally grow through the hierarchical merging of dark-matter halos over cosmic time as expected in the ΛCDM cosmological model (Blumenthal et al. 1984; Davis et al. 1985; Cole et al. 2000). There is, therefore, a clear expectation for galaxy-galaxy and halo-halo merging to be physically linked (Maller et al. 2006; Hopkins et al. 2006; De Lucia & Blaizot 2007). Indeed, modern galaxy formation models predict that massive ellipticals form by major dissipationless (so-called "dry") merging of likewise spheroidal and gas-poor progenitors (Boylan-Kolchin et al. 2006; Naab et al. 2006b), that a large fraction of today's massive ellipticals had their last major merger since redshift $z = 0.5$ (e.g., De Lucia et al. 2006), and that the most-massive systems form at the centers of large dark-matter halos (Dubinski 1998; Aragon-Salamanca et al. 1998). Yet, direct evidence for the major-merger assembly of massive galaxies at present times has been lacking, and finding such systems is needed to place constraints on their rates, progenitor properties, and environmental dependencies. To this end we look for close pairs of massive interacting galaxies within a complete and well-defined sample of over 5000 galaxies with $z \leq 0.12$ and $\mathrm{M_{star}} \geq 5 \times 10^{10}\mathrm{M_{\odot}}$, selected from galaxy groups in the Sloan Digital Sky Survey (SDSS) with dark-matter halo masses above $\mathrm{M_{halo}} = 2.5 \times 10^{13}\mathrm{M_{\odot}}$.

Ellipticals galaxies make up the bulk of the massive end of the red-sequence population with optical

colors indicative of their non-star-forming and old stellar nature. Despite a quiet star-formation history over the last 6–8 billion years (Bell et al. 2005), the total stellar mass density on the red sequence has roughly doubled over this interval (Bell et al. 2004b; Blanton 2006; Borch et al. 2006; Faber et al. 2007; Brown et al. 2007) and now accounts for more than half of the present-day budget (Hogg et al. 2002; Bell et al. 2003), providing strong observational evidence for the ongoing hierarchical growth of the massive galaxy population. These results were derived from red galaxy number densities over a wide range of stellar masses above and below $10^{11}\mathrm{M}_{\odot}$. Owing to the scarcity of the highest-mass galaxies, cosmic variance, and systematic uncertainties in stellar mass estimates, any increase in the number density of $\mathrm{M}_{\mathrm{star}} > 10^{11}\mathrm{M}_{\odot}$ galaxies is poorly constrained, resulting in controversy over whether this population has continued to grow slowly (e.g., Brown et al. 2007) or has been effectively static (e.g., Scarlata et al. 2007), since $z \sim 1$.

Besides number density evolution, mergers of sufficiently massive galaxies could provide a more clear indication for some continued stellar mass growth in the high-mass galaxy population. The existence of a handful of massive red mergers over the redshift interval $0.1 < z < 0.9$ (van Dokkum et al. 1999; Tran et al. 2005; Bell et al. 2006a; Lotz & et al. 2006; Rines et al. 2007) proves that the growth is non-zero at high stellar masses and implies that this mechanism does contribute to the assembly of galaxies at the top of the food chain. Yet, the importance of this process and the related rate of mass growth are highly uncertain given the tiny samples over this large cosmic time interval. Indirect measures such as the presence of faint tidal debris or shells around many local massive ellipticals (van Dokkum 2005; Mihos et al. 2005), the isophotal properties of giant ellipticals (Kang et al. 2007), the lack of evolution of the stellar mass-size relation of red spheroids since $z = 1$ (McIntosh et al. 2005), and the lack of morphological evolution on the red sequence since $z = 0.7$ (Bell et al. 2004a) provide a variety of limits to the importance of dissipationless mergers. Perhaps the most powerful method for obtaining estimates for the stellar mass growth rate via major merging is based on small-scale clustering statistics that provide an accurate measurement of close pair frequencies in real space (Masjedi et al. 2006; Bell et al. 2006b; Masjedi et al. 2007). However, this method likely yields an overestimate of the merger frequency because it assumes that all close pairs will merge. All estimates of merger-driven growth rates are limited by uncertainties in the time interval over which a pair will merge, and over what duration an object could be identified as interacting. Masjedi et al. (2007) find a very small growth rate (1–2% per Gyr) at $z \sim 0.25$ for major mergers involving at least one progenitor drawn from the SDSS Luminous Red Galaxy sample (LRG, Eisenstein et al. 2001); LRGs have typical masses of several times $10^{11}\mathrm{M}_{\odot}$. To date there remains no direct evidence of ongoing merger-driven assembly of massive galaxies at $z < 0.1$, and the LRG result implies that this formation process is no longer important. These facts motivate a thorough search for the existence/nonexistence of ongoing examples in the present-day universe.

While the aforementioned statistical method for finding close physical pairs is powerful, it does not isolate actual merging systems and thus provides no information on the progenitor properties of massive merger remnants. Recent numerical simulations and models make a range of predictions regarding the progenitor morphologies at the time of the last major merger (Khochfar & Burkert 2003; Naab et al. 2006b; Kang et al. 2007), yet robust observational constraints are missing for $\mathrm{M}_{\mathrm{star}} > 10^{11}\mathrm{M}_{\odot}$ systems. Many studies have identified major-merger candidates by either close pairs (Carlberg et al. 1994; Patton et al.

2000; Carlberg et al. 2000; Patton et al. 2002; Bundy et al. 2004; Lin et al. 2004) or disturbed morphologies (Le Fèvre et al. 2000; Conselice et al. 2003; Lotz & et al. 2006), but these samples mostly contain major mergers between lower-luminosity galaxies that tend to be gas-rich spiral disks. Numerical simulations show that such dissipative merging of disk galaxies will not produce massive pressure-supported ellipticals (e.g., Naab et al. 2006a). As mentioned above, only circumstantial evidence and a small number of red galaxy pairs with $z < 0.9$ support the existence of mergers likely to produce massive ellipticals. Our understanding of the progenitors is therefore very limited. Here we present a thorough census of 38 massive merger pairs from SDSS, providing an order-of-magnitude increase in the number of such detections at $z < 0.5$ and allowing an improved understanding of their progenitor properties.

While many estimates of major merger rates are found in the literature, to date no measure of the environmental dependence of merger-driven mass growth has been attempted. In the standard cosmological model, there is a trade off between the expansion of the universe and the gravitational collapse of dark and luminous matter. Therefore, the rate at which stellar mass is assembled at the centers of the largest dark matter halos over recent cosmic history is a fundamental aspect of the ongoing formation of large-scale structure, and the rate that high-mass galaxies form by mergers as a function of halo mass constrains galaxy formation theories. Some theories predict that the mergers producing massive ellipticals occur preferentially in groups rather than in high-density cluster or low-density field environments because the smaller velocity dispersions allow more galaxy interactions (Cavaliere et al. 1992); also dynamical friction is more efficient in lower-mass halos (e.g. Cooray & Milosavljević 2005). Others predict that the brightest cluster galaxies (BCGs) grow by hierarchical merging ("galactic cannibalism") at the centers of the dark-matter potential wells of large clusters (Ostriker & Tremaine 1975; Merritt 1985; Dubinski 1998; Cooray & Milosavljević 2005). A handful of low-redshift BCGs show multiple nuclei suggesting cannibalism in the form of multiple minor mergers (Lauer 1988), but there are no observations of major mergers at the centers of clusters. In this paper we make use of the statistically large SDSS group catalog (Yang et al. 2005; Weinmann et al. 2006) to show that major mergers occur in present-day dense environments, and to explore the halo-mass dependence and central/satellite identity of merger-driven massive galaxy assembly.

Throughout this paper we calculate comoving distances in the ΛCDM concordance cosmology with $\Omega_{\rm m} = 0.3$, $\Omega_\Lambda = 0.7$, and assume a Hubble constant of $H_0 = 70\,{\rm km\,s^{-1}\,Mpc^{-1}}$. SDSS magnitudes are in the AB system.

2. Sample Selection

We make use of public catalogs derived from the SDSS (York et al. 2000) Data Release Two (DR2, Abazajian et al. 2004), which includes spectroscopic and imaging coverage of more than 2600 square degrees. The $ugriz$ passband imaging (Fukugita et al. 1996; Gunn et al. 1998, 2006), precise photometry (Hogg et al. 2001; Smith et al. 2002; Ivezić et al. 2004; Tucker et al. 2006), image processing (Lupton et al. 2002), astrometric calibration (Pier et al. 2003), and spectroscopy (Strauss et al. 2002; Blanton et al. 2003b) of the SDSS provides a powerful database for detailed studies of the galaxy population from the local cos-

mos. We exploit the large-number statistics of the SDSS to search for elusive pairs of massive galaxies undergoing major merging in dense group and cluster environments. As described in detail below, our sample selection consists of (1) a complete and mass-limited set of large dark-matter halos drawn from the SDSS DR2 group catalog[1] (Yang et al. 2005; Weinmann et al. 2006), (2) the subset of massive galaxy pairs within these groups that meet the stellar mass criteria of $\mathrm{M}_1 + \mathrm{M}_2 \geq 10^{11}\mathrm{M}_\odot$, and (3) the identification of merger candidates among the massive pairs.

2.1. Massive Halos from the SDSS Group Catalog

With large surveys of spectroscopic redshifts and imaging data, astronomers are for the first time able to study galaxies according to their membership and position within dark-matter halos (i.e., galaxy groups). Using the halo-based group finder of Yang et al. (2005), Weinmann et al. (2006) extracted groups from an initial sample of 184,425 galaxies with $0.01 \leq z \leq 0.20$ and better than 70% redshift completeness drawn from the New York University Value-Added Galaxy Catalog (NYU-VAGC, Blanton et al. 2005). The NYU-VAGC provides improved processing and additional parameters for the SDSS spectroscopic Main galaxy sample (Strauss et al. 2002), which has an extinction-corrected $r = 17.77$ magnitude limit.

The halo-based group finder of Yang et al. (2005) has been optimized to group galaxies according to their common dark-matter halo, and has been thoroughly tested using mock galaxy redshift surveys. Briefly, the group finder starts with a friends-of-friends algorithm to define potential groups and their centers. Any isolated, bright galaxies not assigned to a potential group are added as likely centers of additional groups. The total group luminosity is converted into an estimate for the group mass using an assumed mass-to-light (M/L) ratio. From this mass estimate, the radius and velocity dispersion of the corresponding dark-matter halo are estimated using the virial equations, which in turn are used to select group members in redshift space. This method is iterated until group memberships converge. In Yang et al. (2005), the performance of this group finder has been tested in terms of completeness of true members and contamination by interlopers, using detailed mock galaxy redshift surveys. The average completeness of individual groups was found to be ~ 90 percent, with only ~ 20 percent interlopers. Furthermore, the resulting group catalogue is insensitive to the initial assumption regarding the M/L ratios.

As described in Weinmann et al. (2006), halo masses for each identified group were estimated using the total group luminosity, $L_{\rm group}$, defined as the summed luminosity of all group members. The motivation behind this is that one naturally expects the group luminosity to be strongly correlated with halo mass. Because of the flux limit of the SDSS, two identical groups observed at different redshifts will have a different $L_{\rm group}$. This bias was circumvented by using $L_{19.5}$ instead, which is defined as the luminosity of all group members brighter than ${}^{0.1}M_r = -19.5 + 5\log h$. The relation between $L_{19.5}$ and $L_{\rm group}$ was calibrated using groups with $z \leq 0.09$, which corresponds to the redshift for which a galaxy with ${}^{0.1}M_r = -19.5 + 5\log h$ has $r = 17.77$, the magnitude limit of the survey. For groups with $z > 0.09$, this 'local'

[1]Public access to the group catalog is at http://www.astro.umass.edu/∼xhyang/Group.html.

calibration between $L_{\rm group}$ and $L_{19.5}$ was used to estimate the latter. Finally, under the assumption that there is a one-to-one relation between $L_{19.5}$ and halo mass, and using the halo mass function corresponding to a flat ΛCDM cosmology with $\Omega_m = 0.3$ and $\sigma_8 = 0.9$, the halo mass of a given group, $\rm M_{halo}$, then follows from matching the number density of groups brighter (in terms of $L_{19.5}$) than the group in consideration to that of halos more massive than $\rm M_{halo}$. Detailed tests with mock galaxy redshift surveys have shown that this method results in group masses that are more reliable than those based on the velocity dispersion of the group members, especially when the number of group members is small.

In Weinmann et al. (2006), this group finder was applied to the NYU-VAGC associated with the SDSS DR2, which yielded halo masses for 53,229 groups spanning $11.8 < \log_{10}(\rm M_{halo}/M_\odot) < 15.5$ and containing 92,315 galaxies. As a result of the method used to assign the group masses, the completeness of the group catalog depends on both halo mass and redshift. In detail, the catalog is complete for groups with $\log_{10}(\rm M_{halo}/M_\odot) > 11.8622$ to $z = 0.06$, $\log_{10}(\rm M_{halo}/M_\odot) > 12.1933$ to $z = 0.12$, and $\log_{10}(\rm M_{halo}/M_\odot) > 13.0877$ to $z = 0.20$.

For our analysis, this group catalog provides two important environmental measures for every member galaxy: (1) an estimate of the virial mass ($\rm M_{halo}$) of the dark-matter halo in which the galaxy resides, and (2) a distinction between central (CEN) and satellite (SAT) galaxies. Throughout, a CEN galaxy is defined as the brightest member of its group. As discussed in detail in Weinmann et al. (2006), these quantities allow more physically-meaningful discussions of the dependencies of galaxy properties on environment than do projected number densities.

We combine two volume-limited samples defined by the halo construction and completeness described above: (I) $0.01 < z \leq 0.06$ and (II) $0.06 < z \leq 0.12$. We exclude halos with $0.12 < z \leq 0.20$ to avoid resolution limitations. At $z = 0.12$, the SDSS resolution of $1.4''$ corresponds to 3 kpc, thus fairly massive galaxies will be only semi-resolved. Moreover, unreliable photometry is known to occur in SDSS for galaxies separated by $< 3''$ (Masjedi et al. 2006), which corresponds to 7–10 kpc over the $0.12 < z \leq 0.20$ interval. We find many close pairs with physical separations less than 10 kpc, thus our redshift cut avoids selecting a large fraction of close pairs with poor photometry. Within the two redshift slices we further limit our selection to halos that have at least three spectroscopic members to allow for a complete search of massive pairs associated with either CEN or SAT galaxies. This restricts our final sample to all SDSS DR2 groups with masses of $\log_{10}(\rm M_{halo}/M_\odot) \geq 13.4$ in volume I, and $\log_{10}(\rm M_{halo}/M_\odot) \geq 13.8$ in II. Hence, our selection is halo mass-limited at values significantly larger than the group catalog completeness limits. We plot the halo mass and redshift distribution of our final sample in Figure 1, which contains 845 groups with masses ranging from one-tenth to ten times that of the Virgo cluster.

2.2. Massive Galaxy Pairs

The primary goal of our study is to find whether evidence exists for the major-merger assembly of massive ($\rm M_{star} > 10^{11} M_\odot$) galaxies in dense environments. We approach this by first inspecting all massive galaxies belonging to the halo mass-limited selection of 845 groups to identify those systems that have a

major companion (mass ratio between 4:1 and 1:1) within a projected separation of 30 kpc. It is important to keep in mind that these companions are neither restricted to be in the SDSS spectroscopic Main sample nor in the group catalog. We then use an image decomposition technique, as described in §2.3, to identify the pairs that exhibit signs of tidal interaction associated with an ongoing merger.

We estimate stellar masses ($\mathrm{M_{star}}$) for all group members using the Bell et al. (2003) stellar M/L ratios as follows:

$$\log_{10}(\mathrm{M_{star}}/\mathrm{M_\odot}) = -0.306 + 1.097^{0.0}(g-r) - 0.15 - 0.4(^{0.0}M_r - 4.67), \quad (1)$$

where the constant 0.15 corrects to a Kroupa (2001) IMF, and $^{0.0}g$ and $^{0.0}r$ are Petrosian magnitudes from the NYU-VAGC (random uncertainties < 0.03 mag) shifted to the $z = 0$ rest-frame using Blanton et al. (2003a) K-corrections and corrected for Milky Way extinction using the Schlegel et al. (1998) dust maps. We subtract 0.1 magnitude to correct for the flux known to be missing from galaxies with early-type morphologies (Blanton et al. 2003c). We use the r-band central-light concentration (R_{90}/R_{50}), defined by the ratio of the radii containing 90% and 50% of the Petrosian flux, to coarsely separate early-type ($R_{90}/R_{50} \geq 2.6$; spheroid-dominated) and late-type ($R_{90}/R_{50} < 2.6$; disk-dominated) galaxies as others have with SDSS data (e.g., Strateva et al. 2001; Hogg et al. 2002; Bell et al. 2003; Kauffmann et al. 2003). The Bell et al. (2003) color-based stellar M/L ratios have 20% random uncertainties and a 0.10-0.15 dex systematic error caused by a combination of effects including dust, stellar population ages, and bursts of star formation. The characteristic stellar mass of the local galaxy mass function from Bell et al. (2003) is $\mathrm{M^*} = 7.24 \times 10^{10}\mathrm{M_\odot}$.

To find major mergers between two galaxies with mass ratios $\leq 4:1$, we start with all 5376 group members more massive than $\mathrm{M_{star}} = 5 \times 10^{10}\mathrm{M_\odot}$ (hereafter **sampM**) and note that this mass limit is the minimum for which an equal-mass merger will produce a $10^{11}\mathrm{M_\odot}$ remnant. We plot the color versus stellar mass distribution of sampM in Figure 2. The contours represent all SDSS DR2 Main galaxies with $z \leq 0.12$. The halo-mass-limited sample of 845 CEN galaxies from sampM are shown as red and blue circles separated by the red/blue sequence boundary from Weinmann et al. (2006), modified to $z = 0$ and $H_0 = 70\,\mathrm{km\,s^{-1}\,Mpc^{-1}}$. The 4531 SATs from sampM are plotted as black solid points. Not surprising, the vast majority of massive galaxies in high-mass groups (both CEN and SAT) have red-sequence colors. We compare the massive galaxy content of sampM with that of the $z \leq 0.12$ DR2 volume in Table 1.

We use the SDSS Image List Tool[2] as a virtual observatory to visually examine an 80×80 kpc region centered on each massive galaxy in sampM, which allows us to view the entire extent of both galaxies in a 30 kpc pair. Although more time-consuming, this method ensures that we find all major companions including those without SDSS spectroscopic data. In addition, our examination allows the identification of individual (non-pair) sources with highly disturbed morphologies suggestive of ongoing major mergers, which cannot be found with automated pair selection. We find seven morphologically-identified mergers that have semi-resolved double nuclei with projected separations too close to be accurately deblended by the SDSS (Fig. 3).

[2]Available from the SDSS SkyServer Tools at http://cas.sdss.org/astro/en/tools/chart/list.asp.

We find that 221 massive galaxies in sampM have a major companion with a projected separation of $d_{12} \leq 30$ kpc (centroid-to-centroid). Operationally, we use an apparent r-band magnitude difference of $|\Delta r_{12}| \leq 1.5$, corresponding to mass ratios $\leq 4:1$ assuming a constant M/L ratio, to identify major companions both with and without spectroscopic data. Throughout this paper we use the following designations for projected pairs: galaxy number 1 is from sampM and galaxy number 2 is its projected companion, regardless of relative brightness or mass. In the cases where both galaxies have spectroscopic redshifts and are massive enough to be included in sampM, galaxy 1 is the primary (i.e., brightest) member and we remove from further analysis the duplicated pair initiated on galaxy number 2. The SDSS spectroscopy is known to be about 8% incomplete overall, independent of galaxy luminosity. The main source of incompleteness results from the $55''$ minimum separation for fiber placement (i.e., "fiber collisions") in the mechanical spectrograph (Blanton et al. 2003b). This selection effect leads to a slight systematic under representation in regions of high galaxy number density (Hogg et al. 2004), such as in massive groups and clusters. Less than one third of the 221 pairs have spectra for both galaxies, and thus, redshifts for galaxies number 1 and 2 (i.e., spec-spec pairs). In what follows we will show that an important fraction of all pair-identified massive mergers have only one spectroscopic progenitor (i.e., spec-phot pairs).

Close pairs of galaxies are used often to infer information about galaxy merging (e.g. Patton et al. 2000; Carlberg et al. 2000; Le Fèvre et al. 2000; Patton et al. 2002; Lin et al. 2004; Bundy et al. 2004; Bell et al. 2006b). These studies use a range of definitions, which usually include tight limits on both velocity and projected spatial separations (typically < 500 km s^{-1} and 10–50 kpc), and do not use further knowledge such as the halo mass or the position relative to the group center. Our choice of $d_{12} \leq 30$ kpc separations is rather arbitrary and we have no way of knowing ab initio whether or not it will include all massive pairs that show obvious signs of interaction. Owing to our larger 80×80 kpc field of view, we effectively search within a projected radius of 40 kpc around each galaxy in sampM, which enable us to find three additional wide-separation ($d_{12} > 30$ kpc) pairs that exhibit strong merging signatures. The maximum projected separation of the additional mergers is 37 kpc. The minute frequency of $30 < d_{12} < 40$ kpc pairs with strong tidal signatures in these groups suggests that wider-separation systems will not be apparent in SDSS-depth imaging data. We include only pairs with $d_{12} \leq 30$ kpc for our projected pair statistics, but include the three additional merger pairs in our progenitor and mass assembly statistics.

Our sample includes three pairs with 2–3$''$ separations, which are a potential source of systematic bias in our major pair selection. As mentioned above, Masjedi et al. (2006) showed that the SDSS photometric pipeline boosts the recovered flux of individual galaxies in very close pairs. For equal-luminosity galaxies separated by 5–20$''$ the excess is only about 5%, but this quickly rises to 20% at $3''$ separation. Moreover, the pipeline has trouble deblending very close pairs as is evident in Figure 3. We do not attempt to separate the progenitors of these mergers, instead we assume that they represent major mergers and explicitly state where we include them in our analysis.

Finally, the subset of 64 major spectroscopic pairs in sampM allow us the unique opportunity to test the frequency of interlopers in massive groups. We find that 25% of the spectroscopic pairs (2 CEN-SAT, 14 SAT-SAT) are comprised of projected galaxies in two separate groups with average absolute velocity separation $\langle|\Delta v|\rangle = 7550$ km s^{-1}. If we limit our analysis to spectroscopic pairs with $d_{12} \leq 30$ kpc and

$\langle|\Delta v|\rangle \leq 500$ km s^{-1}, we find 5% contamination from interlopers in basic agreement with Berrier et al. (2006), who used mock galaxy catalogs from cosmological simulations to demonstrate that 10–50 kpc (14–71 kpc in our assumed cosmology) pairs with less than 500 km s^{-1} separation reside in the same dark-matter halo with a low ($5-20\%$) contamination from projected interlopers. Overall, the spectroscopic pairs from sampM that live in the same group have absolute velocity differences spanning 10 to 1560 km s^{-1} with means of 260 km s^{-1} (CEN-SAT) and 360 km s^{-1} (SAT-SAT). Many of these pairs are likely doomed to merge, yet some may still be chance projections on opposite sides of the same group. We feel that the most conservative approach to locating physically interacting pairs is to look for morphological signs of disturbance, an approach that we adopt and discuss in the next section.

2.3. Identifying Major Mergers

Besides pair statistics, major galaxy mergers are routinely identified by their highly-disturbed appearance (e.g., Le Fèvre et al. 2000; Conselice et al. 2003; Lotz & et al. 2006). Tidal tails and debris, multiple nuclei, strong asymmetries, and other morphological peculiarities are common features in both observations and in simulations of galaxy collisions (Toomre & Toomre 1972; Barnes 1988; Barnes & Hernquist 1992; Dubinski et al. 1996; Barnes & Hernquist 1996; Mihos 2001). Yet, distinguishing major mergers from lower mass ratio "minor" interactions using morphology alone is fraught with uncertainties. For example, depending on the orbital geometry, a 10:1 gas-rich merger can result in a more disturbed morphology than an encounter between two massive ellipticals, which have broad low-surface brightness features (Bell et al. 2006a). We circumvent this issue by selecting major pairs of massive galaxies first, and then fitting symmetric models to the light profiles of each galaxy in each major pair and identifying interaction signatures in the residual (data$-$model) image. Our methodology is similar in spirit to that of Lauer (1986, 1988), who modelled BCGs with multiple nuclei as the line-of-sight superpositions of normal elliptical galaxies.

For each major pair in sampM we use GALFIT (Peng et al. 2002) to fit the surface photometry of both galaxies and any other close companions in the SDSS r-band image data. For each fit we use the global background estimate provided in the SDSS image header. The details of our fitting pipeline developed for SDSS imaging will be presented in Guo et al. (in prep.). Asymmetries commonly associated with galaxy mergers (e.g., tails, bridges, plumes, nonconcentric isophotes, diffuse excess structure, and dynamical friction wakes) are *not well fit* by symmetric models centered on the galaxy. Therefore, to isolate and highlight asymmetries in the residual image we use either a single-component Sérsic or a two-component Sérsic bulge plus exponential disk model for each source, depending on whether or not disk features such as spiral arms, rings, or bars are apparent. We classify any major pair as a merger if there are asymmetric residuals brighter than 24.5 mag arcsec^{-2} associated with *both* progenitor galaxies. All other pairs are deemed non-interacting. This surface brightness limit was used in the selection of SDSS spectroscopic target galaxies (Strauss et al. 2002), and we find that residual features this bright are unambiguous.

For isolated galaxies not undergoing a major interaction, there are a number of other explanations for the presence of asymmetric residual flux, such as lopsided spiral features caused by minor interactions or

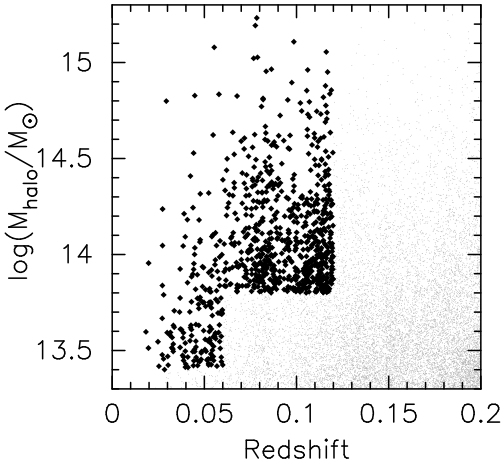

Fig. 1.— Distribution of halo mass and redshift for massive groups identified by Weinmann et al. (2006) in the SDSS DR2. Small grey points show all 12,552 groups with $\mathrm{M_{halo}} > 2 \times 10^{13}\mathrm{M_{\odot}}$; for $z \leq 0.12$ there are 2666 groups above this halo mass cut, the majority of which contain only 1 or 2 spectroscopic members. Black diamonds show our halo-mass and volume-limited selection of 845 groups (see text for details) that we use to search for major pairs of massive galaxies. There are 176 groups with $0.01 < z \leq 0.06$ (vol. I) and $\mathrm{M_{halo}} > 2.5 \times 10^{13}\mathrm{M_{\odot}}$, and 669 with $0.06 < z \leq 0.12$ (vol. II) and $\mathrm{M_{halo}} > 6.3 \times 10^{13}\mathrm{M_{\odot}}$.

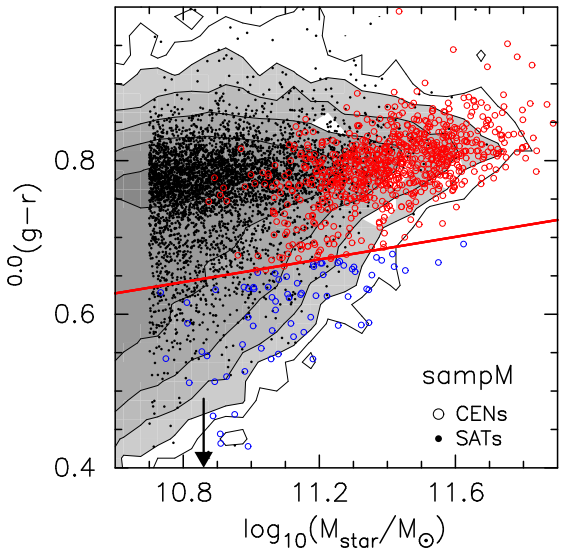

Fig. 2.— Rest-frame optical color versus stellar mass plot for our selection of massive members (sampM) from a halo mass-limited sample of large SDSS DR2 groups. Grayscale contours show all SDSS (DR2) galaxies with $0.01 < z \leq 0.12$; each contour represents a 3-fold increase in the number of galaxies. The solid red line is the red/blue sequence separation we adopt from Weinmann et al. (2006). Blue and red circles denote the subset of 845 CEN galaxies, and black solid points denote the 4531 satellites. The vertical arrow indicates M^* from Bell et al. (2003).

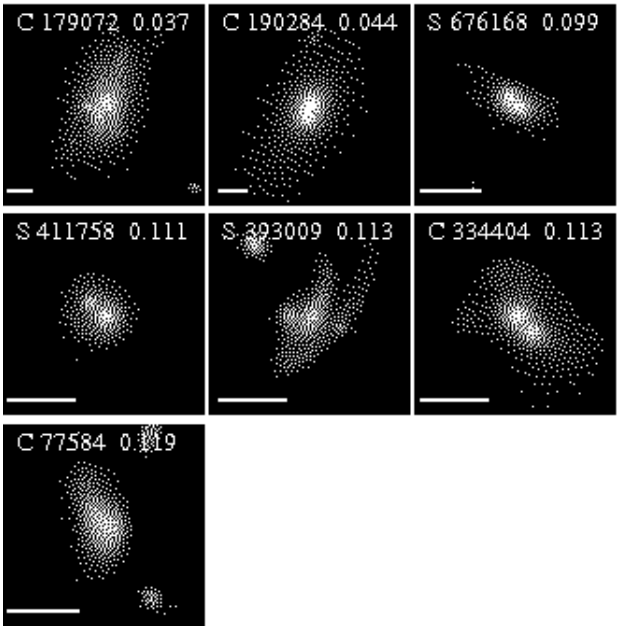

Fig. 3.— Seven additional mergers identified only by strong morphological disturbances, not by close major companions. Images are 60×60 kpc cutouts of gri combined color images with fixed sensitivity scaling downloaded from the SDSS Image List Tool. We distinguish CEN (C) from SAT (S) mergers, and we include the NYU ID and the redshift, at the top of each panel. The horizontal white line shows $10''$ in each panel.

large star-forming regions. The subset of 16 interlopers (§2.2) provides a null sample to demonstrate that no major pairs that are simple line-of-sight projections meet our dual disturbance criteria for identifying mergers. In Figure 4, we show our fitting analysis for two interlopers that have the strongest detectable asymmetries from spiral structure (NYU IDs 95240 and 275580). In each case the asymmetry is associated with only one galaxy of each pair. None of the remaining 14 interloper pairs in Figure 5 exhibit the strong, dual asymmetries that we observe in the merger pairs, which we describe next.

We find 38 pairs of massive galaxies in sampM that we classify as major mergers (35 with $d_{12} \leq 30$ kpc). We display the SDSS r-band image and corresponding GALFIT residual of each merger in increasing redshift order (left to right) in Figures 6 and 7. These images leave little doubt that the two galaxies in each pair are in the midst of merging. We find a variety of strong tidal features including broad tails (e.g., 311008, 352171, and 274752) such as seen during the period between second close passage and final coalescence in dissipationless merger simulations (Naab et al. 2006b) and observations (see Fig. 1, Bell et al. 2006a), and dynamical friction wakes in the outer stellar envelopes (e.g., 367419 and 258681) as predicted by Weinberg (1986) and hinted at in a few BCG systems by (Lauer 1988). In addition, we find bridges (e.g., 301558 and 371303), plumes (e.g., 150206 and 261132), diffuse structure (e.g., 294450 and 9993), and many examples of nonconcentric isophotes (e.g., 392792, 222852, and 373137), which present the strongest indications for tidal contact (Lauer 1988). In Figure 8, we show 10 examples of close (spec-phot) pairs that have no residual asymmetries and are likely the result of chance projections. Comparing these non-interacting examples with the 38 mergers in Figs. 6 & 7 clearly demonstrates the fidelity of our merger identification scheme. As the sensitivity of the SDSS imaging may be too low to detect all interacting pairs of massive galaxies, our classifications provide a conservative lower limit. Nonetheless, our sample identifies the strongest cases and serves as an important dataset for studying the properties of massive merger progenitors in §3.2.

Nearly 70% (26) of these massive mergers have redshift information for only one progenitor (spec-phot pairs) as a result of fiber collisions, which highlights the importance of our thorough approach for identifying such systems. We estimate that we could be missing an additional four (11%) mergers that are photometric-photometric sources based on the 34% (26/76) of progenitor galaxies that have only SDSS photometry. Quantifying the exact number of massive phot-phot mergers in the DR2-based group catalog is beyond the scope of this paper. An improved understanding of the completeness of pairs of merging galaxies in SDSS groups is one of the aims of our next paper.

3. Properties of Massive Mergers in Groups and Clusters

In this section, we explore the properties of the $\mathrm{M_{star}} \geq 10^{11}\mathrm{M_{\odot}}$ mergers that we identified from a complete sample of $\leq 4:1$ mass ratio pairs of massive SDSS galaxies that we selected from group and cluster-sized halos. We compare the distributions of basic observables for merger pairs and major pairs not classified as mergers, quantify the nature of the merger progenitors, make predictions about the remnants, and look for environmental dependencies in this merging population.

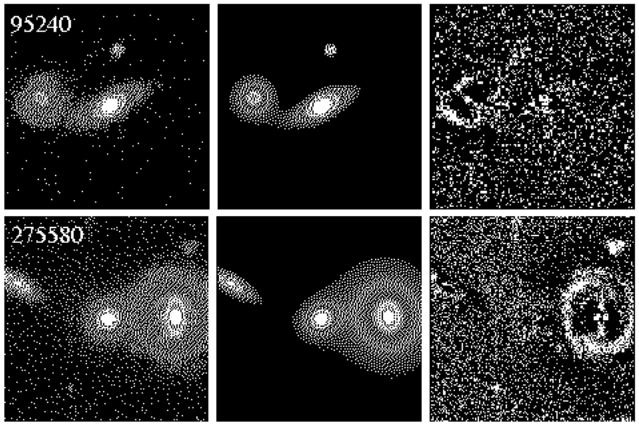

Fig. 4.— Examples of two galaxy pairs with small projected separations but large physical separations; i.e., the two galaxies reside in different groups and are thus not physically associated. *Panels:* (left) r-band SDSS image in arbitrary false-color, logarithmic scale to highlight low-surface brightness features, (middle) GALFIT symmetric model profile, and (right) data−model residual. We identify merging galaxies by the presence of asymmetric residual flux associated with each individual galaxy (see text for details). These two examples are among the subset of 16 null (interloper) cases, none of which meet our merger identification criteria. Some interloper pairs have one galaxy with detectable residuals for a variety of reasons other than an interaction between the two galaxies. We show the strongest residual cases here to illustrate the most-common cause, which is spiral structure. Each image is 80×80 kpc and we provide the NYU-VAGC DR2 identification number (NYU ID) in the upper left.

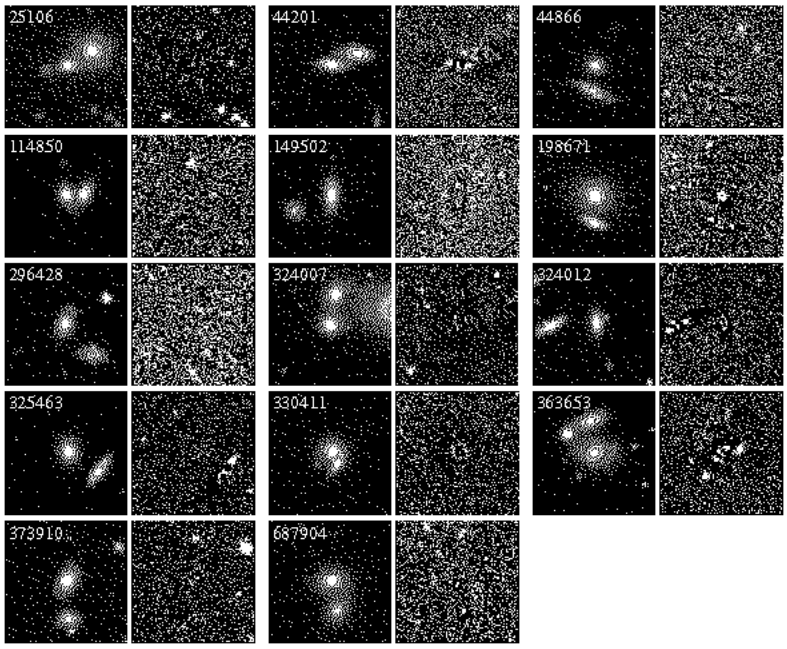

Fig. 5.— The remaining 14 of 16 major pairs that are interlopers (individual galaxies in separate groups). No pair exhibits asymmetric residuals for both galaxies. The images (r-band data and residual with log-scale stretch) are 80×80 kpc and are labeled as in Figure 4.

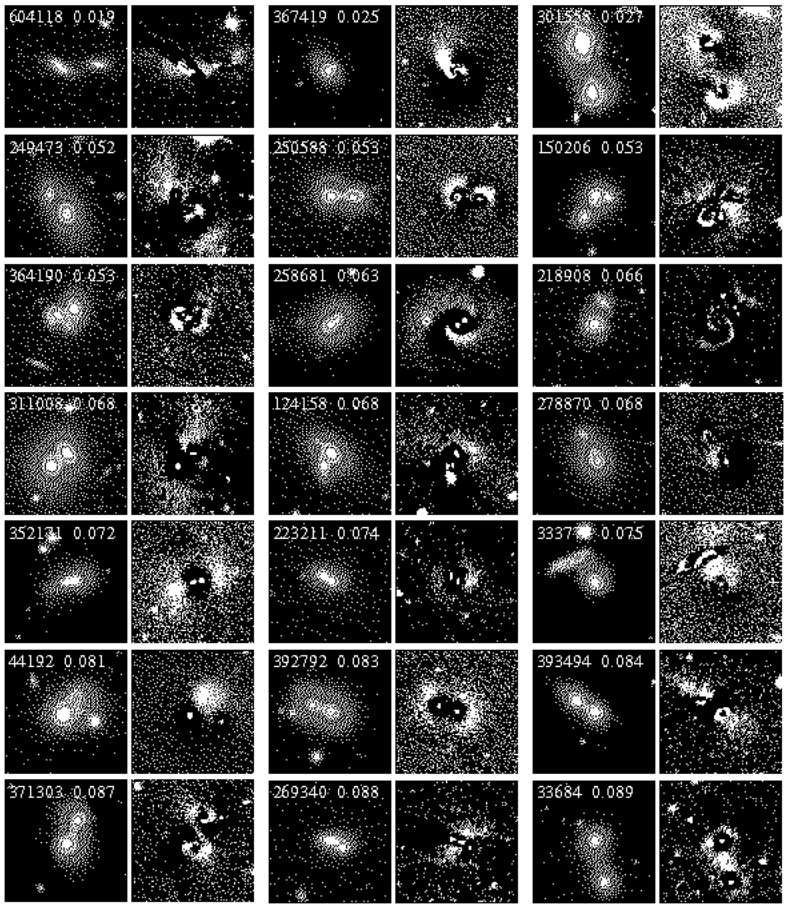

Fig. 6.— See caption for Figure 7.

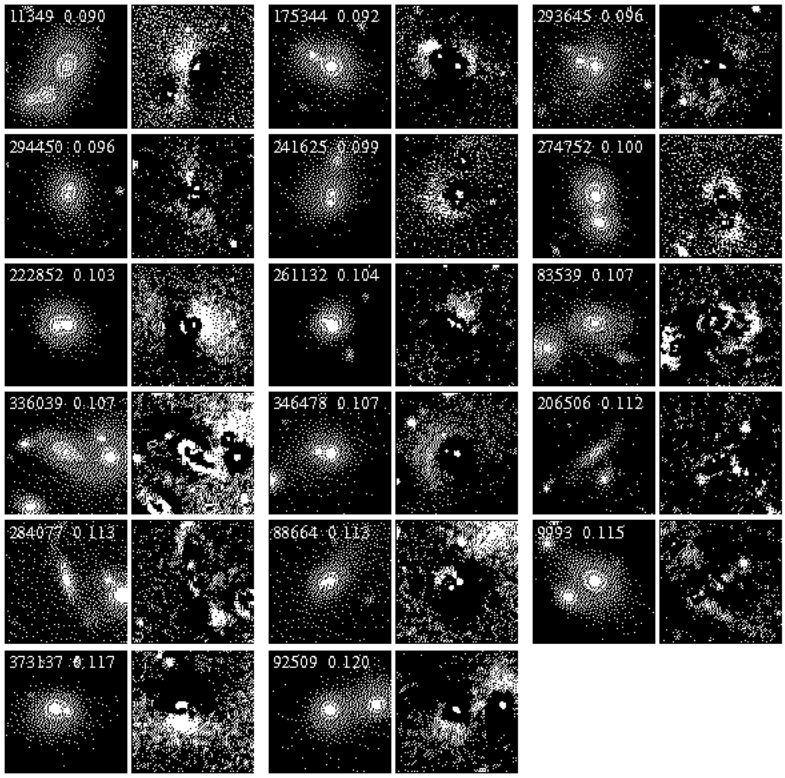

Fig. 7.— The full sample of 38 major-merger pairs of massive galaxies identified in a halo mass-limited subset of SDSS DR2 groups with $z \leq 0.12$ (sampM). Three pairs (301558, 83539, and 284077) have projected separations between $30 < d_{12} < 37$ kpc. We identify these merging systems when both galaxies have asymmetric residual features in excess of 24.5 mag arcsec^{-2}. Such asymmetries are associated with tidal signatures (e.g., tails, bridges, plumes, nonconcentric isophotes, diffuse excess structure, and dynamical friction wakes) of mutual encounters between two galaxies. For each pair we provide the r-band data in false color (arbitrary scaling) at the left, and the data$-$model residual at the right. To highlight low-surface brightness features we Gaussian smoothed (using a 1 pixel sigma) the residual images of each, except for 301558, 250588, 364190, 278870, 352171, 333778, 44192, 392792, 371303, 11349, 241625, and 274752. All images are 80×80 kpc with the NYU ID and spectroscopic redshift given.

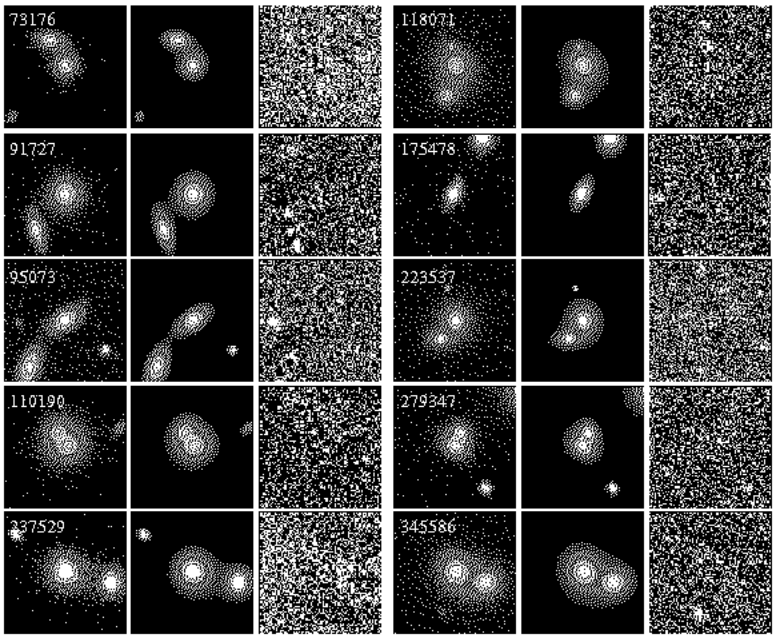

Fig. 8.— Examples of 10 spec-phot pairs in projection that show no signs of disturbance; the central galaxy of each panel has a spectroscopic redshift. These non-interacting pairs likely have much larger physical separations than their projected < 30 kpc separation suggests, and are either interlopers (separate groups) or well-separated within a common halo. All images (r-band data, model, residual with log-scale stretch) are zoomed in to 60×60 kpc, and are labeled as in Figure 4.

3.1. Basic Observables

In Figure 9, we plot the distributions of basic observables that describe each major pair of massive galaxies we selected in §2.2. Here we compare the subsets of 35 mergers ($d_{12} \leq 30$ kpc; bold lines), 16 interlopers (i.e., definite non-interacting; grey bins), and the remaining 170 we classify as non-interacting (thin lines). It is important to note that a simple selection of major pairs of massive galaxies in dense environments yields $< 16\%$ with obvious signs of merger/interaction. We find that the pairs that we identify as mergers have some differences with those without interaction signatures. Likewise, merging galaxies obviously residing in the same group are different from projected pairs of galaxies that reside in distinct host halos.

In general, the merger pairs have a flatter Δr_{12} distribution than non-interacting pairs, with more systems near $\Delta r_{12} = 0$, the proxy for equal-mass mergers, in contrast to the increasing number of non-mergers towards larger magnitude offsets as expected for a simple projected pair sample. Nonetheless, there is no statistical difference between the Δr_{12} distributions of mergers and the subset of known interlopers. Recall that we select pairs with $|\Delta r_{12}| \leq 1.5$, but here we show the Δr_{12} distribution to illustrate that some spec-phot pairs have $\Delta r_{12} > 0$; i.e., the source without SDSS spectroscopy is more massive.

Merging pairs tend to have smaller angular separations $\theta_{\rm sep}$ compared with non-interacting pairs and interlopers. In terms of the colors and concentrations of galaxies in pairs, we find little difference between the interacting and non-interacting subsets. Owing to our selection bias for red galaxies (see Fig. 2) and the stronger clustering of red galaxies (e.g., Zehavi et al. 2002), it is not surprising that the color difference $\Delta(g-r)_{12} = (g-r)_1 - (g-r)_2$ distributions are narrow and peaked near zero. Likewise, given the broad range of concentrations ($2 < R_{90}/R_{50} < 4$) found for SDSS Main galaxies (e.g., Hogg et al. 2002), the relatively small concentration differences $\Delta(R_{90}/R_{50})_{12}$ are consistent with matched morphologies of similarly red galaxies. We note a mild difference between the $\Delta(g-r)_{12}$ and $\Delta(R_{90}/R_{50})_{12}$ distributions of merging and interloper subsets, such that the physically unassociated pairs have an increased chance to be composed of a red massive-group member with a blue, later-type projected companion.

We check whether or not any of the basic pair properties in Figure 9 depend on the redshift z_1 or stellar mass $\rm M_1$ of the pair member from sampM. Only $\theta_{\rm sep}$ depends on z_1, as expected for a sample limited to 30 kpc maximum projected separations. The different subsets (mergers, interlopers, non-interacting) are independent of z_1 and $\rm M_1$, and hence we conclude that the initial selection of sampM did not impart biases on our ability to classify mergers in a larger sample of major pairs. Moreover, despite the differences we find between the observables of merging and non-interacting galaxy pairs, we cannot distinguish different subsets of major pairs based on these differences alone.

As we mentioned in §2.2, a spectroscopic close pair of galaxies that belong to the same host dark-matter halo may reside on opposite sides of the group, and thus have much larger real space separations than their projected separations imply. On the other hand, merger pairs by definition must be in close physical proximity. As such, for pairs where both galaxies are members of the same group, we compare in Figure 10 the merging and non-interacting subsets in terms of their projected spatial (d_{12}) and velocity (v_{12}) separations. We find that the presence/absence of residual asymmetries clearly produces different

d_{12} distributions consistent with the non-interacting pairs being drawn from a much broader distribution of real-space separations than the mergers. Moreover, the declining number of mergers with increasing d_{12} suggests that wider-separation pairs do not typically include tidal distortions that are apparent in the SDSS imaging. Similarly, we find a more narrow distribution of v_{12} for mergers compared to the non-interacting pairs in a matched group, but the significance of this is unclear owing to the large number of spec-phot mergers without z_2 measurements (25 out of 35). There is no substantial difference between $|\Delta r_{12}|$ for the two subsets.

3.2. Nature of Progenitors

In the Introduction, we outlined the importance of improving our understanding of the progenitors of massive mergers. Here we use concentration, rest-frame color, and stellar mass to explore the properties of the progenitor galaxies in our total sample of 38 mergers; we tabulate information for all 76 progenitors in Table 2.

Two thirds of the merger sample have spectroscopic information for only one of the progenitors as a result of fiber collisions (§2.3). To obtain rest-frame quantities for these companions we use K-corrections downloaded from the SDSS PhotoZ table, which we then correct to the redshift of the merger; i.e., we assume $z_2 = z_1$. For all photometric sources in SDSS, PhotoZ provides photometric redshifts $z_{\rm phot}$ and related K-corrections $K(z_{\rm phot})$ to shift quantities to $z = 0$. For our subset of merger pairs we find that $z_{\rm phot}$ is systematically larger than z_1, and thus $K(z_{\rm phot})$ is an overestimate. In the left panel of Figure 11, we show the g and r-band $K(z_{\rm phot})$ bias relative to $K(z_2)$ for the 12 mergers in our sample where we have spectroscopic information for both galaxies. We estimate the correct K-correction for a given passband

$$K(z_2) = K(z_{\rm phot})\frac{\log_{10}(1+z_2)}{\log_{10}(1+z_{\rm phot})}, \tag{2}$$

by assuming $K(z) \propto 2.5\log_{10}(1+z)$ (Blanton et al. 2003a). As we demonstrate in the middle and right panels of Figure 11, our method provides excellent K-correction estimates with a smaller than ± 0.02 mag scatter, a -0.03 mag g-band offset, and no r-band offset. In this manner, we obtain ${}^{0.0}(g-r)$ and $\rm M_{star}$ estimates for each photometric progenitor from its extinction-corrected color downloaded from the SDSS PhotoTag table.

Among the SAT-SAT mergers, there are three spec-phot pairs (336039, 364190, and 373137) where the photometric progenitor is more massive than the host group's central (brightest) galaxy. We, therefore, assume that this galaxy is in fact the CEN and add these pairs to the CEN-SAT merger subset. Our final sample of 38 pairs of massive merging galaxies includes 21 CEN-SAT and 17 SAT-SAT systems. We distinguish between the CEN-SAT and the SAT-SAT mergers in the remaining plots.

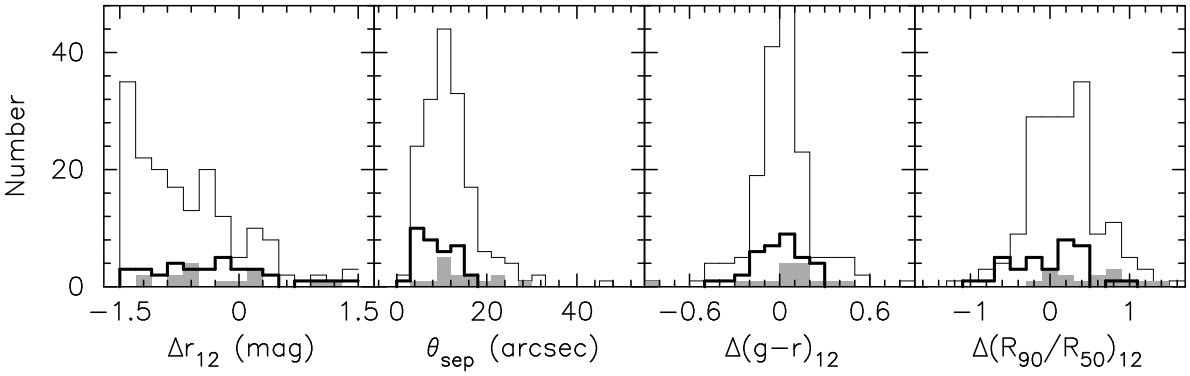

Fig. 9.— Distributions of observables for major ($\leq 4:1$ mass ratio) projected (≤ 30 kpc) pairs split into three subsets: merging/interacting (bold lines), known interlopers (grey bins), and non-interacting systems (thin lines). From left to right we plot the extinction-corrected r-band Petrosian magnitude difference, angular separation, extinction-corrected $(g-r)$ Petrosian color difference, and r-band concentration difference. All parameter differences are defined $\Delta p = p_1 - p_2$ such that 1 denotes the galaxy from sampM and 2 denotes the companion.

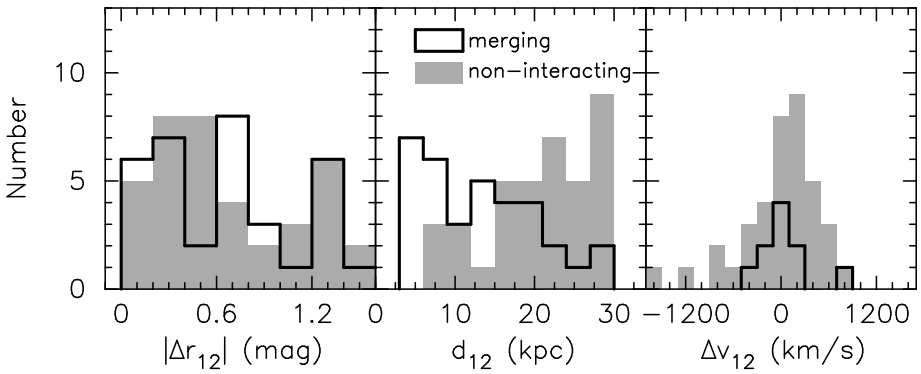

Fig. 10.— Comparison of the properties of 35 major-merging (bold lines) and 39 non-interacting (grey bins) galaxy pairs where both galaxies belong to the same host halo. From left to right, the relative properties of progenitor galaxies 1 and 2 are absolute value of the r-band magnitude difference, projected spatial separation in kiloparsecs, and velocity difference. Only 10 of the 35 major interacting pairs with $d_{12} \leq 30$ kpc have spectroscopic information for both progenitors to enable the calculation of Δv.

3.2.1. Progenitor Morphology

We explore the color and concentration of the progenitor galaxies in massive merger pairs in Figure 12. In the left panel, we plot the rest-frame color of progenitor number 2 relative to the blue/red sequence boundary shown in Figure 2 as a function of the color of progenitor number 1 from sampM for each merger pair. The data points in both panels of Figure 12 are color-coded to distinguish blue or red-sequence ${}^{0.0}(g-r)_1$ colors, and data above the dashed line have red ${}^{0.0}(g-r)_2$ colors. We find that $90 \pm 5\%$ of the massive mergers we identify are comprised of two red progenitors; only one merger is blue-blue and three are mixed pairs. In the right panel, we show the central-light concentration of progenitor 2 plotted against that of progenitor 1. Consistent with the high fraction of red-red mergers, $92 \pm 4\%$ of the mergers are comprised of two concentrated progenitors with $R_{90}/R_{50} > 2.6$, the fiducial value for early-type morphologies (see §2.2). Three mergers are made up of an early/late mix according to concentration, with one of each red-red, red-blue, and blue-blue.

The nature of the progenitors appears to depend little on whether the merger is positioned at the center of the host group or is between a pair of SAT galaxies. Owing to the small-number statistics, the slight decrease in the red-red merger fractions from 95% (CEN-SAT) to 82% (SAT-SAT), and likewise for early-early mergers from 95% (CEN-SAT) to 88% (SAT-SAT), are consistent with no difference. Generally speaking, the major mergers that will produce $\mathrm{M_{star}} > 10^{11}\mathrm{M_{\odot}}$ remnants in massive groups are between two red-sequence spheroids that have little cold gas for star formation and are presumably dissipationless. The properties of these low-redshift mergers match the six $0.1 < z < 0.9$ dissipationless mergers in Bell et al. (2006a).

3.2.2. Progenitor Mass Ratios

The major mergers we have identified are drawn from pairs with $|\Delta r_{12}| \leq 1.5$ mag, our proxy for 4:1 to 1:1 mass ratios (§2.2). Here, we explore the actual stellar mass ratios of the merger progenitors. Overall, the Petrosian color-derived $\mathrm{M_{star}}$ estimates for sampM are well-behaved as demonstrated by the tight red-sequence of CEN and SAT members in Figure 2. We note, however, that there are a handful of extreme outliers in color-mass space such that some massive group galaxies have very red colors, especially at the high-mass tip of the red sequence. Large systematic errors in color translate into errors in $\mathrm{M_{star}}$, which is a critical issue when trying to ascertain the progenitor mass ratios. Nevertheless, it is unclear whether the measured colors are the result of an error in the photometric pipeline or simply the intrinsic nature of a rare population.

We attempt to quantify the amplitude of systematic uncertainties in our stellar mass estimates from issues related to the SDSS photometry by recomputing $\mathrm{M_{star}}$ for all 76 merger progenitors using SDSS Model[3] magnitudes in place of Petrosian quantities in (1). In Figure 13, we plot the relative difference

[3]In addition to standard Petrosian magnitudes, the SDSS photometry includes measures of galaxy flux from the best-fit model, either a de Vaucouleurs or an exponential, to the r-band image profile.

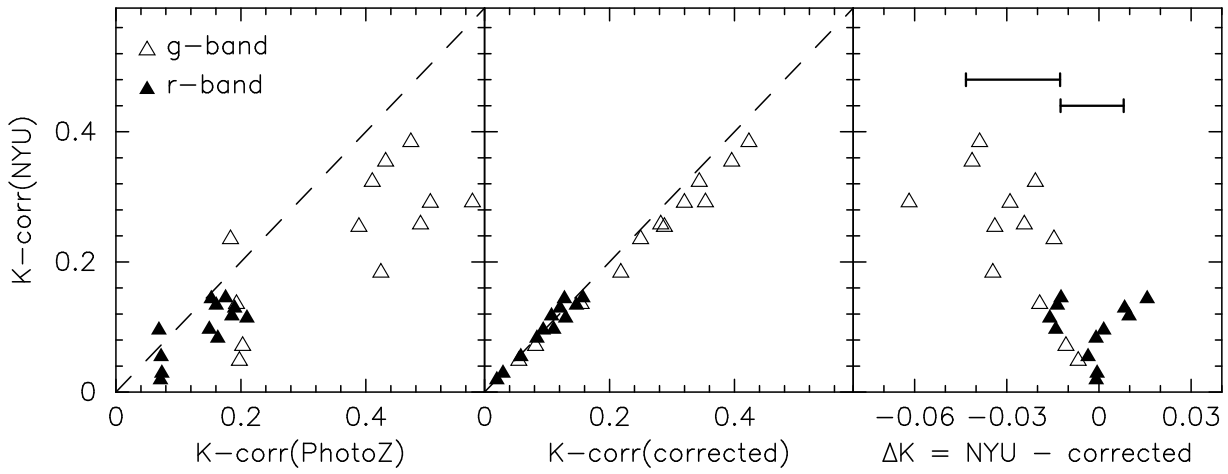

Fig. 11.— K-corrections for g (open triangles) and r (solid triangles) passbands shifted to $z = 0$ for the subset of 12 companion galaxies in major-merger pairs where spectroscopic redshifts are available for both progenitors. We plot the accurate NYU_VAGC K-corrections versus those from PhotoZ (left), corrected using (2) (middle), and the relative difference between the NYU_VAGC and our corrected values (right); the error bars show the mean and scatter of the offsets in each passband.

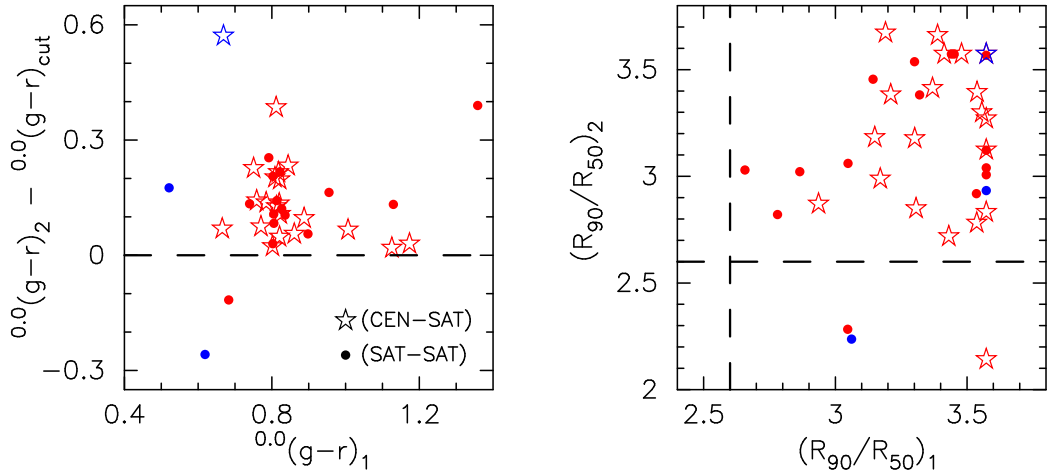

Fig. 12.— Colors and concentrations of the progenitors of massive major mergers. Mergers involving a CEN and SAT galaxy (stars) are distinguished from those involving two SATs (circles). Data points are color-coded to represent blue/red sequence color of the progenitor in sampM (galaxy number 1). *Left:* relative rest-frame $(g-r)$ color of the companion galaxy (number 2) with respect to the blue/red cut plotted as a function of progenitor number 1 color. Red points above the dashed line represent red-red mergers. *Right:* r-band central-light concentrations of progenitor 2 versus progenitor 1. Dashed lines show the crude early/late morphology cut of $R_{90}/R_{50} = 2.6$.

between the masses derived with each type of magnitude as a function of the ${}^{0.0}M_r$ and ${}^{0.0}(g-r)$ differences (Petrosian-Model), and $\theta_{\rm sep}$. We find that the bulk (75%) of the progenitors have a small (≤ 0.15 dex) but systematic shift towards lower masses, which correlates with fainter ${}^{0.0}M_r$, when using Model magnitudes. This subset has a tight locus of $\Delta[{}^{0.0}(g-r)]$ comparable to the quoted ~ 0.04 mag random error for Petrosian colors. The remaining 25% of the progenitors have systematic color offsets as large as $+0.30(-0.25)$ mag resulting in a greater than factor of 2 shift in $\rm M_{star}$, or more than twice as much as the expected 0.10-0.15 dex systematic uncertainty (§2.2). In Table 2, we note the progenitors with ≥ 0.3 dex difference between their Petrosian and Model-based $\rm M_{star}$ estimates. We find no dependence of these mass offsets on CEN versus SAT, nor on the angular separation of the pairs. One possible explanation for the large photometric variances could be related to known pipeline errors for very close pairs (Masjedi et al. 2006), yet very few of our projected pair sample have $\theta_{\rm sep} < 3''$ and it is difficult to understand how close pairs would have boosted flux in one passband (r) but not another (g) to account for the very red colors.

We plot the color-stellar-mass distribution of the 76 progenitors in Figure 14 using symbols to represent the Petrosian-derived values and arrows to explicitly show the direction and amplitude of the shifts to Model-derived values in this parameter space. We note that the extremely-red outliers in Petrosian space have Model colors more in accord with normal red galaxies. Generally speaking, most of the progenitors occupy the massive end of the red sequence; 80% have $\rm M_{star} > 10^{11} M_{\odot}$. This means that some very massive galaxies continue to be assembled in the low-redshift universe. Yet, as a result of selection effects, we cannot determine the significance of the small number of progenitors with $\rm M_{star} < 10^{11} M_{\odot}$. The selection of sampM creates a bias insofar as the percent contribution of massive halo members to the overall DR2 galaxy population in the $z \leq 0.12$ volume decreases significantly as a function of stellar mass (see Table 1). In other words, our halo mass-limited selection misses vast numbers of galaxies with $\rm M_{star} < 10^{11} M_{\odot}$ simply because they live in halos with $\rm M_{halo} < 2.5 \times 10^{13} M_{\odot}$. The importance of massive major mergers in lower-mass halos will be the subject of a followup paper.

In Figure 15, we show the stellar mass ratios of the progenitors in our sample of mergers as a function of the mass $\rm M_1$ of the progenitor drawn from sampM. There is little qualitative difference between the distributions of $\rm M_1/M_2$ based on Petrosian or Model photometry. Both CEN-SAT and SAT-SAT mergers have mass ratios mostly between 2:1 and 1:1, with the primary progenitors in central mergers tending toward higher masses than those in SAT-SAT mergers. We discuss the implications of these mass ratios on the merger assembly of massive galaxies in §4.1.

3.2.3. The Predicted Color-Mass Distribution of Massive Remnants

Recall that besides the sample of 38 merger pairs we have also identified seven massive mergers based on their disturbed morphologies (§2.2; Fig. 3). Under the assumption that these morphologically-identified mergers are examples of an advanced evolutionary stage between interacting pairs of massive galaxies and

the final coalesced remnant[4], it is worthwhile to compare their positions in the color-stellar-mass plane with the predicted locations for the remnants of the merger pairs. For each pair of progenitors we calculate the remnant's final mass $\mathrm{M_{rem}} = \mathrm{M_p} + f\mathrm{M_s}$ and its mass-weighted color

$$(g-r)_{\mathrm{rem}} = -2.5\log_{10}\left[\frac{\mathrm{M_p}}{\mathrm{M_{rem}}}10^{-0.4(g-r)_{\mathrm{p}}} + \frac{f\mathrm{M_s}}{\mathrm{M_{rem}}}10^{-0.4(g-r)_{\mathrm{s}}}\right], \quad (3)$$

where the primary progenitor is more massive than the secondary by definition (i.e., $\mathrm{M_p} \geq \mathrm{M_s}$). The factor f allows us to adjust the fraction of the secondary progenitor's initial mass that is included in $\mathrm{M_{rem}}$. In what follows we use Petrosian-based quantities.

In each panel of Figure 16 we show the seven morphologically-identified mergers as squares with CEN (SAT) examples distinguished by open (closed) symbols. Six of the seven have red-sequence colors, and all CENs are more massive than the SATs. We first compare the color-mass distribution of these mergers with the predict distribution of remnants from the 38 merger pairs under the simple assumption that the total mass of the secondary is always accreted onto the remnant ($f = 1$). Nearly all remnants have red-sequence colors reflecting the nature of their progenitors. In terms of the stellar masses of the observed mergers compared to the predicted remnants, we find better agreement with SATs than for CENs. Three quarters of the future remnants at the centers of massive groups are more massive than the four morphologically-identified CEN mergers. With small number statistics it is difficult to make definitive comparisons. It is possible that the time interval that a late-stage merger is apparent depends on stellar mass, such that higher-mass mergers coalesce into a single object faster. Another possibility is that some mass is lost during the merging process.

Zibetti et al. (2005) found that the intracluster light (ICL) within 100 kpc of the group or cluster center makes up as much as 40% of the total cluster luminosity (galaxies+ICL), and they showed that the stars making up the ICL have the same colors as the old-stellar light from the massive galaxies in the intracluster environment. Therefore, it is conceivable that some stellar mass from the massive, red, CEN-SAT mergers deep in the potential wells of large groups and clusters winds up in the ICL rather than as part of the central remnant galaxy. Various groups have argued that disruption of SAT galaxies through tidal stripping and heating can remove 10–80% of their stellar mass and account for the ICL (Monaco et al. 2006; White et al. 2007; Conroy et al. 2007). These theories provide a way to reconcile the predicted merger-driven mass growth above $10^{11}\mathrm{M_\odot}$ in a ΛCDM cosmology with the little growth that is observed in the stellar mass function (e.g., Wake et al. 2006; Brown et al. 2007). In the right panel of Figure 16, we try a highly conservative test of the latter scenario by assuming $f = 0.5$ for CEN-SAT remnants, but $f = 1$ for SAT-SAT mergers. This assumption implies that each massive SAT merging with the center of its host potential well would lose 50% of its present stellar mass by the time it coalesced from an average projected group-centric distance of 15 kpc. In the previous section, we show that these CEN-SAT mergers have mass ratios typically within a factor of two of unity, and these systems are clearly separated by distances much less than the ICL half-light radius. These facts suggest either (i) a much lower SAT mass loss than our conservative assumption, or (ii) the SAT masses at the ICL half-light radius were in excess of the CEN with which they

[4]This is a fair assumption given that all seven morphologically-disturbed mergers have stellar masses in excess of $10^{11}\mathrm{M_\odot}$.

will eventually merge. Another possibility is that the CEN-SAT masses are much more disparate as a result of the standard SDSS photometry systematically underestimating the CEN luminosities (Lauer et al. 2007). Resolving these issues is beyond the scope of this paper. Instead we simply point out that in terms of relative stellar mass from SDSS photometry, we see better agreement between the observed mergers and the predicted remnants at the centers of massive groups if we assume that only half of the SAT mass ends up in the remnant, which suggests that major mergers at the bottom of the potential well in groups and clusters could be an important source for the ICL.

3.3. Environmental Dependencies

One of the key goals of our study is to quantify the environmental dependencies, if any, of massive mergers. Here we use the host's halo mass, and the distinction between CEN (brightest) and SAT members, to explore the environments of the mergers that we have identified in large SDSS groups and clusters from the local universe. In what follows, we consider the combined sample of 45 massive mergers: 38 close pairs identified by residual asymmetric structure plus seven single sources identified by their morphologically-disturbed appearance.

3.3.1. Preference for Central Merging

We find that the centers of massive groups and clusters appear to be the preferred environment for the major-merger assembly of present-day $\mathrm{M_{star}} > 10^{11}\mathrm{M_{\odot}}$ galaxies. More than half of the mergers we identify involve the central (most-luminous) member of the host dark-matter halo, yet there are five times less CENs than SATs to merge with in sampM. Thus, on average, 3% of massive groups with $z \leq 0.12$ have a major merger, but less than 1% of all massive galaxies within these groups are merging.

In Figure 17, we compare the group-centric properties of the CEN and SAT mergers. We find that mergers involving a CEN are significantly closer to the luminosity-weighted center of their host group than mergers between SAT galaxies. The average projected group-centric distance of CEN mergers is 210 kpc, compared to 490 kpc for SATs. Moreover, relative to the luminosity-weighted group redshifts, the CEN mergers have a narrower distribution of velocity offsets ($\sigma = 200$ km s^{-1}) than the SAT mergers ($\sigma = 370$ km s^{-1}). The small group-centric offsets of the CEN mergers are consistent with them residing at the bottom of their halo's potential well, where dynamical friction is maximum. In contrast, most merging SATs have large group-centric offsets as expected given their rank within their host group. At face value, these results indicate that mergers between massive SATs do occur, yet in terms of their morphologies (Fig.12) and mass ratios (Fig.15) there are no clear differences between CEN-SAT and SAT-SAT merger progenitors.

A merger between two massive galaxies likely occurs at the dynamical center of a common dark-matter halo. If the merger is between two SATs, then we may be witnessing a merger at the center of a subhalo that

merged with the larger host halo[5]. Another possibility is that the SAT merger represents the true dynamical center of the host halo. Indeed, we find that 20% (4/20) of the SAT mergers reside closer to the center of the group's projected galaxy distribution than the spectroscopic CEN galaxy identified by the group catalog, and have a total stellar mass estimate $\mathrm{M_1 + M_2}$ that is greater than the mass of the CEN ($\mathrm{M_{CEN}}$). We identify these four pairs in Table 2 and explore their inclusion/exclusion in the CEN-SAT merger subset in our analyzes of central merger frequencies and mass accretion rates in the following sections.

It is also possible that a significant fraction of the SAT mergers are at the center of a distinct halo seen in projection along the line of sight to the host halo. This explanation would explain the group-centric differences in Figure 17, and the similarities in color, concentration, and mass ratios that we observe. We note that 6/20 SAT mergers have $\mathrm{M_1 + M_2 \geq M_{CEN}}$ and large projected group-centric distances, providing circumstantial evidence for membership in a separate group from the host of the CEN galaxy. Yet, a simple calculation shows that there is only a 10% chance for a line-of-sight projection of a distinct group with $\mathrm{M_{halo} \geq 10^{13} M_\odot}$ within 1 Mpc radius and ± 400 km s^{-1} depth (following the group-centric properties of the SAT-SAT mergers in Fig. 17). This estimate is an upper limit based on the mean number density of groups that typically host a $\mathrm{10^{11} M_\odot}$ CEN galaxy ($10^{-3.5}$ Mpc^{-3}, Mo & White 2002), and the assumption that the correlation strength between groups increases the local density relative to the mean by a factor of 10. Therefore, our observed frequency of 3% of groups with central mergers implies that we should find only three SAT-SAT mergers that are misidentified CEN-SAT systems from a projected group. We find 16–20 SAT-SAT mergers in 845 groups (1.9–2.4% depending on whether we consider the four mentioned above to be at the center of their host), indicating that most are correctly identified as SAT-SAT interactions. Given the large velocity dispersions of high-density environments, true SAT-SAT mergers are not expected. While we do find large group-centric velocity offsets for SAT-SAT mergers (Fig. 17), for the subset of 12 spec-spec mergers we find no significant difference between the small velocity separations (v_{12}, see Fig. 10) of CEN-SAT and SAT-SAT mergers. Therefore, we tentatively conclude that massive SAT-SAT mergers identify the centers of large subhalos that have recently accreted onto their host.

3.3.2. Merging Dependence on Halo Mass

By identifying the massive galaxy mergers in a halo mass-limited selection of large groups, we can for the first time constrain their importance as a function of halo mass. In the left panel of Figure 18, we plot the halo-mass dependence for the frequency of groups that have merger-driven assembly of $\mathrm{M_{star} \geq 10^{11} M_\odot}$ galaxies restricted to group centers. We find that the fraction of groups that have a massive merger at their center (bold red line) is statistically constant at 3% over the interval $13.4 < \log_{10}(\mathrm{M_{halo}/M_\odot}) < 14.9$; we note that including the four morphologically-identified CEN mergers plus the four misclassified SAT-SAT mergers at their host's dynamical center results in a minor increase to this frequency (thin red line, open diamonds). We contrast our estimate for the merger frequency dependence on halo mass, based

[5]The halo-based group finder of Yang et al. (2005) used to produce the SDSS group catalog does not have the ability to distinguish subhalos within the halo defining each galaxy group.

solely on galaxies exhibiting obvious tidal features, to that obtained from simple close projected pairs of massive galaxies (dashed black line), which grows steadily with halo mass as a result of the increased projected number density of massive galaxies in dense environments. The increased chance of projection with increasing $\mathrm{M_{halo}}$ also occurs for the subset of spec-spec pairs that are found in the same host group (solid black line), but the amplitude is diminished owing to the high spectroscopic incompleteness in the pairs that we study. At $\log_{10}(\mathrm{M_{halo}}/\mathrm{M_{\odot}}) < 14.6$, the number of spec-spec projected pairs in matched halos is less than that of all mergers, which by definition must reside in the same host halo, because the latter include spec-phot pairs.

In the right panel of Figure 18, we repeat our analysis of merger and projected pair frequencies as a function of halo mass using the combined CEN-SAT plus SAT-SAT sample. When considering all possible mergers that will produce high-mass remnants (red lines), the frequency is roughly constant at 5% for $13.4 < \log_{10}(\mathrm{M_{halo}}/\mathrm{M_{\odot}}) < 14.9$. Including/excluding the seven non-pair mergers (morphologically-identified) does not change these frequencies significantly. The issues with using simple projected pair statistics (black lines) to estimate merger frequencies grow rapidly out of hand for massive groups that contain large numbers of $\mathrm{M_{star}} \geq 5 \times 10^{10}\mathrm{M_{\odot}}$ galaxies; e.g., on average nearly half of all $\log_{10}(\mathrm{M_{halo}}/\mathrm{M_{\odot}}) = 14.5$ groups have one major pair of massive galaxies that appear close in projection.

Besides merger frequency per group we can approach massive mergers from a different perspective and calculate the frequency of $\mathrm{M_{star}} \geq 5 \times 10^{10}\mathrm{M_{\odot}}$ SATs that are currently involved in a merger that can be identified as such with the technique that we use here. We calculate separate frequencies for merging with a CEN or another massive SAT galaxy in bins of halo mass, and plot them in Figure 19. As a function of $\mathrm{M_{halo}}$, the SAT merging frequencies decrease from a few percent for our lowest-mass groups, to $\leq 1\%$ for groups larger than $\mathrm{M_{halo}} = 5 \times 10^{13}\mathrm{M_{\odot}}$. The CEN-SAT merging follows a very similar decreasing frequency trend with increasing $\mathrm{M_{halo}}$ as SAT-SAT mergers, which is qualitatively consistent with dynamical friction and provides more circumstantial evidence that SAT-SAT mergers are occurring at the dynamical centers of recently accreted subhalos. Even though SATs have a large relative velocity dispersion, they can still merger through dynamical friction if they are both members of a subhalo.

4. Discussion

We find the first direct observational evidence for an important population of galaxy-galaxy mergers with total stellar masses above $10^{11}\mathrm{M_{\odot}}$ in the local universe. These objects provide an unprecedented census of the progenitor properties for the merger-driven assembly of high-mass galaxies, which we compare to recent predictions from numerical models of galaxy formation and evolution. Moreover, the existence of these mergers prove that a measurable amount of stellar mass growth continues in the massive galaxy population at present times, and we compare estimates based on this sample with other estimates in the literature. Finally, we have identified mergers restricted to reside in large SDSS groups and clusters with $z \leq 0.12$, thus allowing the first constraints on the halo-mass dependencies of recent massive merger activity. While it is well-established that massive galaxies are more common in such high-density environments, we

are missing much more than 50% of the population with $\mathrm{M_{star}} < 4 \times 10^{11}\mathrm{M_{\odot}}$ in the local volume, as Table 1 shows. Therefore, we must keep this caveat in mind when interpreting the conditions for which our results hold. In an upcoming study, we are examining the role of major mergers as a function of stellar mass over the full range of environments hosting galaxies more massive than $\mathrm{M_{star}} = 5 \times 10^{10}\mathrm{M_{\odot}}$.

4.1. Massive Merger Progenitors: Observations Meet Theories

Establishing the luminosity dependence of elliptical (E) galaxy properties (Davies et al. 1983; Bender 1988; Bender et al. 1992) set the stage for theories regarding the types of merger progenitors that would produce the characteristics of low and high-mass early-type galaxies (ETGs)[6] galaxies (Bender et al. 1992; Kormendy & Bender 1996; Faber et al. 1997). We concentrate on modern numerical simulations and semi-analytic models that attempt to reproduce the kinematic, photometric, and structural properties observed in massive Es through major merging (Naab et al. 1999; Naab & Burkert 2003; Khochfar & Burkert 2003, 2005; Naab et al. 2006b; Boylan-Kolchin et al. 2006; Kang et al. 2007). For this discussion we make the straight-forward assumption that the major mergers that we have identified will produce remnants that are *not unlike* the $\mathrm{M_{star}} > 10^{11}\mathrm{M_{\odot}}$ galaxy population already in place. We can only guess at remnant properties (see Fig. 16), but in general, massive galaxies on the red-sequence are typically early-type.

As we show in Figure 15, the progenitor masses are comparable for the most part, and quantitatively consistent with the LRG-LRG merger mass spectrum from Masjedi et al. (2007) under the assumption that companions merge on dynamical friction time scales. N-body simulations (e.g. Naab et al. 1999) have long shown that $\mathrm{M_1/M_2} \approx 1$ are necessary to produce the lack of significant rotation observed in massive Es. Yet, a near unity mass ratio alone is not sufficient to produce the predominance of boxy and anisotropic Es found at high luminosity (Naab & Burkert 2003; Naab et al. 2006b). To match the decreasing fraction of rotational support and increasing fraction of boxiness in more luminous Es, the role of gas dissipation must be significantly reduced at high masses (Bender et al. 1992; Khochfar & Burkert 2005; Naab et al. 2006a; Kang et al. 2007), and recent ETG-ETG merger simulations have demonstrated this numerically (Naab et al. 2006b). Figures 12 and 14 show that 90% of the progenitors in this study have concentrated light profiles and red-sequence colors, both common attributes of ETGs, with little or no cold gas content. In addition, the tidal signatures of the bulk of these massive mergers (see Figs. 6 & 7) match those of observed (Bell et al. 2006a) and simulated (Naab et al. 2006b) major dissipationless (or gas-poor) merging of ETGs. Thus, our sample represents a more than order-of-magnitude increase in the number of such known systems with $z < 0.2$, and demonstrates that dissipationless merging is indeed an important channel for the formation of massive galaxies.

Finally, we compare the observed high fraction of ETG-ETG mergers ($f_{\mathrm{ETG-ETG}} = 0.9$) with several semi-analytic predictions. Recall that we have looked for signs of interaction in > 200 major pairs from a

[6]The distinction between elliptical and early-type galaxies is often blurred in the literature. We consider Es to be a morphological subset of ETGs, which are concentrated and spheroid-dominated systems including Es, lenticulars (S0s), and Sa spirals. When referencing other authors we remain faithful to their choice of nomenclature.

total sample of > 5000 massive galaxies (i.e., sampM), yet only 10% of the 38 mergers we identify could possibly form a $\mathrm{M_{star}} > 10^{11}\mathrm{M_{\odot}}$ remnant by other than an ETG-ETG merger. The progenitor morphologies of this study best match the predictions of Khochfar & Burkert (2003), who find $f_{\mathrm{E-E}} = 0.75$ for the last major merger of $4L^{*}$ remnants, independent of environment. We find much larger ETG-ETG fractions than Naab et al. (2006b) who predict only 20-35% (also independent of environment) over the estimated mass range of our merger remnants ($11.1 < \log_{10}(\mathrm{M_{star}}/\mathrm{M_{\odot}}) < 11.7$), and Kang et al. (2007) who predict $f_{\mathrm{ETG-ETG}} < 0.1$ for $\log_{10}(\mathrm{M_{star}}/\mathrm{M_{\odot}}) > 11$. We note that these predicted progenitor morphologies for present-day Es are based on the final major mergers that could occur over a large redshift range out to $z \sim 1$, which could be different in nature to those that occur in the short time interval that we observe. Moreover, we focus on high-density environments known to have very few massive late-type (blue) galaxies (Butcher & Oemler 1978), which might explain the low number of "mixed" (early-late or elliptical-spiral) mergers that we find. Hence, for these models to be consistent with our data, either (1) the $f_{\mathrm{ETG-ETG}}$ of present-day major mergers depends on halo mass (i.e., environment), or (2) the relative importance of major mixed mergers has decreased significantly since $z = 1$.

4.2. Estimating Stellar Mass Accretion Rates

The existence of massive dissipationless mergers at low redshift is direct observational evidence that the growth of $\mathrm{M_{star}} > 10^{11}\mathrm{M_{\odot}}$ galaxies continues at present times in agreement with many cosmologically-motivated simulations (Khochfar & Burkert 2005; De Lucia et al. 2006; Kaviraj & et al. 2007; Kang et al. 2007). Moreover, even under conservative assumptions that limit the amount of companion mass that is added to massive CEN galaxies, all of our sample will still result in remnants with $\mathrm{M_{star}} > 10^{11}\mathrm{M_{\odot}}$. Previously, the observational evidence for recent merger-based assembly of $z \sim 0$ massive Es was limited to luminous/massive galaxy clustering statistics (Masjedi et al. 2006; Bell et al. 2006b; Masjedi et al. 2007) or post-merger signatures that cannot distinguish between minor and major merging; e.g., tidal shells (Malin & Carter 1983), fine structure (Schweizer & Seitzer 1992), faint tidal features (van Dokkum 2005; Mihos et al. 2005), or kinematic/photometric properties (e.g., Kang et al. 2007). With the merger sample presented here we can quantify directly the amount of growth, occurring in dense environments, at the high-mass end of the stellar mass function.

Going from the observed merger counts to an inferred merger rate is limited mostly by the uncertainty in the merger timescale (t_{merg}) that one assumes. Numerical models show that the time interval for two galaxies to interact and finally merge into a single remnant depends critically on the orbital parameters, progenitor mass ratios and densities, and the degree to which the merger is dissipationless. For major mergers of massive galaxies a number of different t_{merg} have been put forth in the literature based on simple orbital timescale arguments. For example, Masjedi et al. (2006) derived a reasonable lower limit of $t_{\mathrm{merg}} = 0.2$ Gyr for a close ($d_{1,2} = 10$ kpc) pair of LRG galaxies with a velocity dispersion of $\sigma = 200$ km s^{-1}. Naturally, bound pairs with $d_{1,2} > 10$ kpc separation will take longer to merge. Bell et al. (2006b) made a similar calculation for somewhat less-massive galaxies typically separated by $d_{1,2} = 15$ kpc and estimated $t_{\mathrm{merg}} = 0.4$ Gyr and argued for at least a factor of two uncertainty in this time. The mergers

in this study have an average projected separation of 15.5 kpc (see Fig. 10), so in what follows, we adopt $t_{\rm merg} = 0.4^{+0.4}_{-0.2}$ Gyr with conservative error bars that encompass the range of uncertainties discussed in the literature.

Here, we compute the rate of stellar mass accretion by major merging onto massive galaxies in large groups. First, we find that the total mass accreted onto the centers of the $N_{\rm CEN} = 845$ halos that we study is $\sum f{\rm M_{s},}_i = 3.9(3.5) \times 10^{12}{\rm M}_\odot$, if we include (exclude) the four SAT-SAT mergers at their host's dynamical center (see §3.3.1). ${\rm M_{s},}_i$ is the stellar mass of the secondary (SAT) galaxy in the $i^{\rm th}$ CEN-SAT merger, and f is the fraction of ${\rm M_{s},}_i$ that winds up as part of the CEN galaxy. The rate of stellar mass buildup per massive CEN galaxy is therefore

$$\dot{\rm M}_{\rm CEN} = \frac{\sum f{\rm M_{s},}_i}{N_{\rm CEN}} \times \frac{1}{t_{\rm merg}}, \tag{4}$$

or between $1.0^{+1.0}_{-0.5} \times 10^{10}{\rm M}_\odot{\rm Gyr}^{-1}$ and $1.2^{+1.1}_{-0.6} \times 10^{10}{\rm M}_\odot{\rm Gyr}^{-1}$, depending on which sample of CEN-SAT mergers that we consider. The lopsided error bars result from the range of accretion rates for $t_{\rm merg} = 0.4^{+0.4}_{-0.2}$ Gyr, as described above. If we divide all of these accretion rates by $2.69 \times 10^{11}{\rm M}_\odot$, the average stellar mass of the 845 CEN galaxies in this study, we find that each CEN is growing by 1–9% per Gyr. Finally, these values can be decreased by assuming $f < 1$ in (4), but as we discuss in §3.2.3, $f = 0.5$ represents a likely lower limit.

Likewise, the total stellar mass accreted onto all galaxies in sampM is $\sum f{\rm M_{s},}_i + \sum {\rm M_{s},}_j = 5.1 \times 10^{12}{\rm M}_\odot$, where ${\rm M_{s},}_j$ is the mass of the secondary (SAT) galaxy in the $j^{\rm th}$ SAT-SAT merger. Therefore, the growth per ${\rm M_{star}} \geq 5 \times 10^{10}{\rm M}_\odot$ galaxy in high-mass groups is

$$\dot{\rm M}_{(\geq 5\times10^{10}{\rm M}_\odot)} = \frac{\sum f{\rm M_{s},}_j + \sum {\rm M_{s},}_j}{(N_{\rm CEN} + N_{\rm SAT} - N_{\rm s,sampM})} \times \frac{1}{t_{\rm merg}}, \tag{5}$$

where $N_{\rm s,sampM} = 12$ is the number of secondary SAT galaxies in sampM that are involved in major mergers and must be subtracted to avoid double counting. We find $\dot{\rm M}_{(\geq 5\times10^{10}{\rm M}_\odot)} = 2.4^{+2.4}_{-1.2} \times 10^9{\rm M}_\odot{\rm Gyr}^{-1}$; if we assume $f = 0.5$ for CEN-SAT mergers only we find $\dot{\rm M}_{(\geq 5\times10^{10}{\rm M}_\odot)} = 1.6^{+1.5}_{-0.7} \times 10^9{\rm M}_\odot{\rm Gyr}^{-1}$. Given that the average stellar mass of sampM galaxies is $1.04 \times 10^{11}{\rm M}_\odot$, we find that every massive galaxy is growing by 1–5% per Gyr. Even though SAT-SAT mergers may occur as frequently as CEN-SAT mergers in these massive groups, the centers are where much of the mass growth takes place. It is clear from Figure 15 that mostly only ${\rm M_{star}} > 10^{11}{\rm M}_\odot$ galaxies build up in mass by major mergers in groups with ${\rm M_{halo}} > 2.5 \times 10^{13}{\rm M}_\odot$. In contrast, we find few mergers among the $5 \times 10^{10} < {\rm M_{star}} < 10^{11}{\rm M}_\odot$ galaxies in these high-mass groups, which make up the bulk (60%) of sampM. This suggests that if major merging is playing an important role in the strong mass growth observed on the red sequence below M* (Bell et al. 2004b; Blanton 2006; Borch et al. 2006; Faber et al. 2007; Brown et al. 2007), it is occurring in lower-mass groups than we study here.

Rather than mass growth rates we can use the same line of reasoning to estimate massive galaxy-galaxy merging rates of $(21 + 4)/845/t_{\rm merg} = 0.074^{+0.074}_{-0.037}{\rm Gyr}^{-1}$ for CEN-SAT and $(38 + 7)/(845 + 4531 - 12)/t_{\rm merg} = 0.021^{+0.021}_{-0.011}{\rm Gyr}^{-1}$ for all galaxies in sampM. For these estimates we included the seven additional major mergers (4 CEN, 3 SAT) we identified by their highly-disturbed appearance. Masjedi et al.

(2006) found a strict upper limit to the LRG-LRG rate of only $0.006\mathrm{Gyr}^{-1}$. We estimate that LRGs have a stellar mass range of $11.4 < \log_{10}(\mathrm{M_{star}}/\mathrm{M_{\odot}}) < 12.0$, based on typical red-sequence colors and luminosities between $4L^*$ and $25L^*$. Within these mass limits, we find a merger rate of $5/462/t_{\mathrm{merg}} = 0.027^{+0.027}_{-0.014}\mathrm{Gyr}^{-1}$ on the red sequence, or 2–9 times the LRG-LRG rate. In Table 1, we show that the high-mass groups that we study contain $> 70\%$ of the very-massive, red galaxy population in the $z \leq 0.12$ volume of DR2, with the vast majority being CENs. Yet, the same group selection contains only 30% of the population of $11.4 < \log_{10}(\mathrm{M_{star}}/\mathrm{M_{\odot}}) < 11.6$ systems. These numbers show that a significant portion of the local counterparts to LRGs are found in groups with $\mathrm{M_{halo}} < 2.5 \times 10^{13}\mathrm{M_{\odot}}$. Therefore, we conclude that LRG-LRG merging occurs more frequently in the more massive groups.

5. Summary

Using the SDSS DR2 group catalog we probe a sufficiently large enough volume of the low-redshift universe to identify major mergers that will produce $\mathrm{M_{star}} \geq 10^{11}\mathrm{M_{\odot}}$ galaxies in large groups and clusters. We find 45 massive mergers in a complete sample of more than 5000 galaxies with $\mathrm{M_{star}} \geq 5\times10^{10}\mathrm{M_{\odot}}$ that reside in 845 groups with $\mathrm{M_{halo}} > 2.5 \times 10^{13}\mathrm{M_{\odot}}$. We identify 38 pairs of merging galaxies such that both systems exhibit asymmetric features consistent with mutual tidal interactions, and another seven mergers that have disturbed morphologies and semi-resolved double nuclei. This work provides the first direct evidence for present-day massive mergers, and complements existing studies at higher redshifts (van Dokkum et al. 1999; Bell et al. 2006a; Lotz & et al. 2006; Rines et al. 2007). With this sample, we provide new empirical constraints on the progenitor nature, the environmental dependence, and the stellar mass growth rate of merger-driven assembly of high-mass galaxies. We summarize our results as follows:

- Mergers, as defined here, make up only 16% of the major pairs of massive galaxies with a maximum projected separation of 30 kpc.
- An important percentage (70%) of these mergers would be lost in an automated search of spec-spec pairs as a result of the known spectroscopic incompleteness of the SDSS in dense environments.
- 90% of the mergers are between two red-sequence galaxies with concentrated (spheroid-dominated) morphologies, and broad tidal asymmetries like those seen in observations and in simulations of major dissipationless merging of spheroidal galaxies (Naab et al. 2006b; Bell et al. 2006a).
- Two thirds of the mergers have progenitor mass ratios of 1:1 to 2:1, despite a complete search of major pairs down to 4:1, indicating that near equal-mass merging is preferred in high-density environments.
- Mergers at the centers of massive groups are more common than between two SAT galaxies, but the latter are also identified and are morphologically indistinguishable from CEN-SAT mergers. We argue that SAT-SAT mergers could identify the dynamical centers of large subhalos that have recently been accreted by their host halo, rather than the centers of distinct halos seen in projection.

- The frequency that massive SATs have a major merger with a more-massive CEN or SAT galaxy decreases with halo mass in a manner that is qualitatively consistent with the expectations of dynamical friction.
- Based on reasonable assumptions, the centers of massive halos in the present-day universe are growing in stellar mass by 1–9% per Gyr on average, through major mergers as we observe here.
- Red galaxies with $\mathrm{M_{star}} \geq 2.5 \times 10^{11}\mathrm{M_{\odot}}$, which are comparable to LRGs, merge with their counterparts in these high-mass groups at a rate that is 2–9 times higher than that found for all LRG-LRG merging by Masjedi et al. (2006).

It is becoming clear that gas-poor, major merging between massive red and bulge-dominated galaxies is an important mechanism for producing the most-massive galaxies. Using the SDSS we have demonstrated that the centers of dark-matter halos are the preferred environment for building these giants. Moreover, this analysis shows that our technique for identifying such mergers is very promising for future studies of much larger samples.

We made extensive use of the SDSS SkyServer Tools (http://cas.sdss.org/astro/en/tools/). Thanks to discussions with Chien Peng, Martin Weinberg, Eric Bell, and Yu Lu. D. H. M. and N. K. acknowledge support from the National Aeronautics and Space Administration (NASA) under LTSA Grant NAG5-13102 issued through the Office of Space Science. Funding for the SDSS has been provided by the Alfred P. Sloan Foundation, the Participating Institutions, the National Aeronautics and Space Administration, the National Science Foundation, the U.S. Department of Energy, the Japanese Monbukagakusho, and the Max Planck Society. The SDSS Web site is http://www.sdss.org/. The SDSS is managed by the Astrophysical Research Consortium (ARC) for the Participating Institutions, which are The University of Chicago, Fermilab, the Institute for Advanced Study, the Japan Participation Group, The Johns Hopkins University, Los Alamos National Laboratory, the Max-Planck-Institute for Astronomy (MPIA), the Max-Planck-Institute for Astrophysics (MPA), New Mexico State University, University of Pittsburgh, Princeton University, the United States Naval Observatory, and the University of Washington. This publication also made use of NASA's Astrophysics Data System Bibliographic Services.

REFERENCES

Abazajian, K., Adelman-McCarthy, J. K., Agüeros, M. A., Allam, S. S., Anderson, K. S. J., Anderson, S. F., Annis, J., Bahcall, N. A., Baldry, I. K., Bastian, S., & et al. 2004, AJ, 128, 502

Aragon-Salamanca, A., Baugh, C. M., & Kauffmann, G. 1998, MNRAS, 297, 427

Barnes, J. E. 1988, ApJ, 331, 699

Barnes, J. E., & Hernquist, L. 1992, ARA&A, 30, 705

—. 1996, ApJ, 471, 115

Bell, E. F., McIntosh, D. H., Barden, M., Wolf, C., Caldwell, J. A. R., Rix, H.-W., Beckwith, S. V. W., Borch, A., Häussler, B., Jahnke, K., Jogee, S., Meisenheimer, K., Peng, C., Sanchez, S. F., Somerville, R. S., & Wisotzki, L. 2004a, ApJ, 600, L11

Bell, E. F., McIntosh, D. H., Katz, N., & Weinberg, M. D. 2003, ApJS, 149, 289

Bell, E. F., Naab, T., McIntosh, D. H., Somerville, R. S., Caldwell, J. A. R., Barden, M., Wolf, C., Rix, H.-W., Beckwith, S. V., Borch, A., Häussler, B., Heymans, C., Jahnke, K., Jogee, S., Koposov, S., Meisenheimer, K., Peng, C. Y., Sanchez, S. F., & Wisotzki, L. 2006a, ApJ, 640, 241

Bell, E. F., Papovich, C., Wolf, C., Le Floc'h, E., Caldwell, J. A. R., Barden, M., Egami, E., McIntosh, D. H., Meisenheimer, K., Pérez-González, P. G., Rieke, G. H., Rieke, M. J., Rigby, J. R., & Rix, H.-W. 2005, ApJ, 625, 23

Bell, E. F., Phleps, S., Somerville, R. S., Wolf, C., Borch, A., & Meisenheimer, K. 2006b, ApJ, 652, 270

Bell, E. F., Wolf, C., Meisenheimer, K., Rix, H.-W., Borch, A., Dye, S., Kleinheinrich, M., Wisotzki, L., & McIntosh, D. H. 2004b, ApJ, 608, 752

Bender, R. 1988, A&A, 193, L7

Bender, R., Burstein, D., & Faber, S. M. 1992, ApJ, 399, 462

Berrier, J. C., Bullock, J. S., Barton, E. J., Guenther, H. D., Zentner, A. R., & Wechsler, R. H. 2006, ApJ, 652, 56

Blanton, M. R. 2006, ApJ, 648, 268

Blanton, M. R., Brinkmann, J., Csabai, I., Doi, M., Eisenstein, D., Fukugita, M., Gunn, J. E., Hogg, D. W., & Schlegel, D. J. 2003a, AJ, 125, 2348

Blanton, M. R., Hogg, D. W., Bahcall, N. A., Baldry, I. K., Brinkmann, J., Csabai, I., Eisenstein, D., Fukugita, M., Gunn, J. E., Ivezić, Ž., Lamb, D. Q., Lupton, R. H., Loveday, J., Munn, J. A., Nichol, R. C., Okamura, S., Schlegel, D. J., Shimasaku, K., Strauss, M. A., Vogeley, M. S., & Weinberg, D. H. 2003b, ApJ, 594, 186

Blanton, M. R., Hogg, D. W., Bahcall, N. A., Brinkmann, J., Britton, M., Connolly, A. J., Csabai, I., Fukugita, M., Loveday, J., Meiksin, A., Munn, J. A., Nichol, R. C., Okamura, S., Quinn, T., Schneider, D. P., Shimasaku, K., Strauss, M. A., Tegmark, M., Vogeley, M. S., & Weinberg, D. H. 2003c, ApJ, 592, 819

Blanton, M. R., Schlegel, D. J., Strauss, M. A., Brinkmann, J., Finkbeiner, D., Fukugita, M., Gunn, J. E., Hogg, D. W., Ivezić, Ž., Knapp, G. R., Lupton, R. H., Munn, J. A., Schneider, D. P., Tegmark, M., & Zehavi, I. 2005, AJ, 129, 2562

Blumenthal, G. R., Faber, S. M., Primack, J. R., & Rees, M. J. 1984, Nature, 311, 517

Borch, A., Meisenheimer, K., Bell, E. F., Rix, H.-W., Wolf, C., Dye, S., Kleinheinrich, M., Kovacs, Z., & Wisotzki, L. 2006, A&A, 453, 869

Boylan-Kolchin, M., Ma, C.-P., & Quataert, E. 2006, MNRAS, 369, 1081

Brown, M. J. I., Dey, A., Jannuzi, B. T., Brand, K., Benson, A. J., Brodwin, M., Croton, D. J., & Eisenhardt, P. R. 2007, ApJ, 654, 858

Bundy, K., Fukugita, M., Ellis, R. S., Kodama, T., & Conselice, C. J. 2004, ApJ, 601, L123

Burstein, D., Bender, R., Faber, S., & Nolthenius, R. 1997, AJ, 114, 1365

Butcher, H., & Oemler, A. 1978, ApJ, 219, 18

Carlberg, R. G., Cohen, J. G., Patton, D. R., Blandford, R., Hogg, D. W., Yee, H. K. C., Morris, S. L., Lin, H., Hall, P. B., Sawicki, M., Wirth, G. D., Cowie, L. L., Hu, E., & Songaila, A. 2000, ApJ, 532, L1

Carlberg, R. G., Pritchet, C. J., & Infante, L. 1994, ApJ, 435, 540

Cavaliere, A., Colafrancesco, S., & Menci, N. 1992, ApJ, 392, 41

Cole, S., Lacey, C. G., Baugh, C. M., & Frenk, C. S. 2000, MNRAS, 319, 168

Conroy, C., Wechsler, R. H., & Kravtsov, A. V. 2007

Conselice, C. J., Bershady, M. A., Dickinson, M., & Papovich, C. 2003, AJ, 126, 1183

Cooray, A., & Milosavljević, M. 2005, ApJ, 627, L85

Cox, T. J., Dutta, S. N., Di Matteo, T., Hernquist, L., Hopkins, P. F., Robertson, B., & Springel, V. 2006, ApJ, 650, 791

Davies, R. L., Efstathiou, G., Fall, S. M., Illingworth, G., & Schechter, P. L. 1983, ApJ, 266, 41

Davis, M., Efstathiou, G., Frenk, C. S., & White, S. D. M. 1985, ApJ, 292, 371

De Lucia, G., & Blaizot, J. 2007, MNRAS, 375, 2

De Lucia, G., Springel, V., White, S. D. M., Croton, D., & Kauffmann, G. 2006, MNRAS, 366, 499

Dressler, A. 1980, ApJ, 236, 351

Dubinski, J. 1998, ApJ, 502, 141

Dubinski, J., Mihos, J. C., & Hernquist, L. 1996, ApJ, 462, 576

Eisenstein, D. J., Annis, J., Gunn, J. E., Szalay, A. S., Connolly, A. J., Nichol, R. C., Bahcall, N. A., Bernardi, M., Burles, S., Castander, F. J., Fukugita, M., Hogg, D. W., Ivezić, Ž., Knapp, G. R., Lupton, R. H., Narayanan, V., Postman, M., Reichart, D. E., Richmond, M., Schneider, D. P., Schlegel, D. J., Strauss, M. A., SubbaRao, M., Tucker, D. L., Vanden Berk, D., Vogeley, M. S., Weinberg, D. H., & Yanny, B. 2001, AJ, 122, 2267

Faber, S. M., Tremaine, S., Ajhar, E. A., Byun, Y., Dressler, A., Gebhardt, K., Grillmair, C., Kormendy, J., Lauer, T. R., & Richstone, D. 1997, AJ, 114, 1771

Faber, S. M., Willmer, C. N. A., Wolf, C., Koo, D. C., Weiner, B. J., Newman, J. A., Im, M., Coil, A. L., Conroy, C., Cooper, M. C., Davis, M., Finkbeiner, D. P., Gerke, B. F., Gebhardt, K., Groth, E. J., Guhathakurta, P., Harker, J., Kaiser, N., Kassin, S., Kleinheinrich, M., Konidaris, N. P., Kron, R. G., Lin, L., Luppino, G., Madgwick, D. S., Meisenheimer, K., Noeske, K. G., Phillips, A. C., Sarajedini, V. L., Schiavon, R. P., Simard, L., Szalay, A. S., Vogt, N. P., & Yan, R. 2007, ApJ, 665, 265

Fukugita, M., Ichikawa, T., Gunn, J. E., Doi, M., Shimasaku, K., & Schneider, D. P. 1996, AJ, 111, 1748

Gunn, J. E., Carr, M., Rockosi, C., Sekiguchi, M., Berry, K., Elms, B., de Haas, E., Ivezić, Ž., Knapp, G., Lupton, R., Pauls, G., Simcoe, R., Hirsch, R., Sanford, D., Wang, S., York, D., Harris, F., Annis, J., Bartozek, L., Boroski, W., Bakken, J., Haldeman, M., Kent, S., Holm, S., Holmgren, D., Petravick, D., Prosapio, A., Rechenmacher, R., Doi, M., Fukugita, M., Shimasaku, K., Okada, N., Hull, C., Siegmund, W., Mannery, E., Blouke, M., Heidtman, D., Schneider, D., Lucinio, R., & Brinkman, J. 1998, AJ, 116, 3040

Gunn, J. E., Siegmund, W. A., Mannery, E. J., Owen, R. E., Hull, C. L., Leger, R. F., Carey, L. N., Knapp, G. R., York, D. G., Boroski, W. N., Kent, S. M., Lupton, R. H., Rockosi, C. M., Evans, M. L., Waddell, P., Anderson, J. E., Annis, J., Barentine, J. C., Bartoszek, L. M., Bastian, S., Bracker, S. B., Brewington, H. J., Briegel, C. I., Brinkmann, J., Brown, Y. J., Carr, M. A., Czarapata, P. C., Drennan, C. C., Dombeck, T., Federwitz, G. R., Gillespie, B. A., Gonzales, C., Hansen, S. U., Harvanek, M., Hayes, J., Jordan, W., Kinney, E., Klaene, M., Kleinman, S. J., Kron, R. G., Kresinski, J., Lee, G., Limmongkol, S., Lindenmeyer, C. W., Long, D. C., Loomis, C. L., McGehee, P. M., Mantsch, P. M., Neilsen, Jr., E. H., Neswold, R. M., Newman, P. R., Nitta, A., Peoples, J. J., Pier, J. R., Prieto, P. S., Prosapio, A., Rivetta, C., Schneider, D. P., Snedden, S., & Wang, S.-i. 2006, AJ, 131, 2332

Hashimoto, Y., & Oemler, A. J. 1999, ApJ, 510, 609

Hogg, D. W., Blanton, M., Strateva, I., Bahcall, N. A., Brinkmann, J., Csabai, I., Doi, M., Fukugita, M., Hennessy, G., Ivezić, Ž., Knapp, G. R., Lamb, D. Q., Lupton, R., Munn, J. A., Nichol, R., Schlegel, D. J., Schneider, D. P., & York, D. G. 2002, AJ, 124, 646

Hogg, D. W., Blanton, M. R., Brinchmann, J., Eisenstein, D. J., Schlegel, D. J., Gunn, J. E., McKay, T. A., Rix, H.-W., Bahcall, N. A., Brinkmann, J., & Meiksin, A. 2004, ApJ, 601, L29

Hogg, D. W., Finkbeiner, D. P., Schlegel, D. J., & Gunn, J. E. 2001, AJ, 122, 2129

Hopkins, P. F., Hernquist, L., Cox, T. J., Di Matteo, T., Robertson, B., & Springel, V. 2006, ApJS, 163, 1

Ivezić, Ž., Lupton, R. H., Schlegel, D., Boroski, B., Adelman-McCarthy, J., Yanny, B., Kent, S., Stoughton, C., Finkbeiner, D., Padmanabhan, N., Rockosi, C. M., Gunn, J. E., Knapp, G. R., Strauss, M. A., Richards, G. T., Eisenstein, D., Nicinski, T., Kleinman, S. J., Krzesinski, J., Newman, P. R., Snedden, S., Thakar, A. R., Szalay, A., Munn, J. A., Smith, J. A., Tucker, D., & Lee, B. C. 2004, Astronomische Nachrichten, 325, 583

Kang, X., van den Bosch, F. C., & Pasquali, A. 2007, MNRAS, 808

Kauffmann, G., Heckman, T. M., White, S. D. M., Charlot, S., Tremonti, C., Peng, E. W., Seibert, M., Brinkmann, J., Nichol, R. C., SubbaRao, M., & York, D. 2003, MNRAS, 341, 54

Kaviraj, S., & et al. 2007, submitted, (astro-ph/0709.0806)

Khochfar, S., & Burkert, A. 2003, ApJ, 597, L117

—. 2005, MNRAS, 359, 1379

Kormendy, J., & Bender, R. 1996, ApJ, 464, L119+

Kroupa, P. 2001, MNRAS, 322, 231

Lauer, T. R. 1986, ApJ, 311, 34

—. 1988, ApJ, 325, 49

Lauer, T. R., Faber, S. M., Richstone, D., Gebhardt, K., Tremaine, S., Postman, M., Dressler, A., Aller, M. C., Filippenko, A. V., Green, R., Ho, L. C., Kormendy, J., Magorrian, J., & Pinkney, J. 2007, ApJ, 662, 808

Le Fèvre, O., Abraham, R., Lilly, S. J., Ellis, R. S., Brinchmann, J., Schade, D., Tresse, L., Colless, M., Crampton, D., Glazebrook, K., Hammer, F., & Broadhurst, T. 2000, MNRAS, 311, 565

Lin, L., Koo, D. C., Willmer, C. N. A., Patton, D. R., Conselice, C. J., Yan, R., Coil, A. L., Cooper, M. C., Davis, M., Faber, S. M., Gerke, B. F., Guhathakurta, P., & Newman, J. A. 2004, ApJ, 617, L9

Lotz, J., & et al. 2006, ApJ submitted, (astro-ph/0602088)

Lupton, R. H., Ivezic, Z., Gunn, J. E., Knapp, G., Strauss, M. A., & Yasuda, N. 2002, 4836, 350

Malin, D. F., & Carter, D. 1983, ApJ, 274, 534

Maller, A. H., Katz, N., Kereš, D., Davé, R., & Weinberg, D. H. 2006, ApJ, 647, 763

Masjedi, M., Hogg, D. W., & Blanton, M. 2007, ApJ submitted, (astro-ph/0708.3240)

Masjedi, M., Hogg, D. W., Cool, R. J., Eisenstein, D. J., Blanton, M. R., Zehavi, I., Berlind, A. A., Bell, E. F., Schneider, D. P., Warren, M. S., & Brinkmann, J. 2006, ApJ, 644, 54

McIntosh, D. H., Bell, E. F., Rix, H.-W., Wolf, C., Heymans, C., Peng, C. Y., Somerville, R. S., Barden, M., Beckwith, S. V. W., Borch, A., Caldwell, J. A. R., Häußler, B., Jahnke, K., Jogee, S., Meisenheimer, K., Sánchez, S. F., & Wisotzki, L. 2005, ApJ, 632, 191

Merritt, D. 1985, ApJ, 289, 18

Mihos, J. C. 2001, ApJ, 550, 94

Mihos, J. C., Harding, P., Feldmeier, J., & Morrison, H. 2005, ApJ, 631, L41

Mo, H. J., & White, S. D. M. 2002, MNRAS, 336, 112

Monaco, P., Murante, G., Borgani, S., & Fontanot, F. 2006, ApJ, 652, L89

Naab, T., & Burkert, A. 2003, ApJ, 597, 893

Naab, T., Burkert, A., & Hernquist, L. 1999, ApJ, 523, L133

Naab, T., Jesseit, R., & Burkert, A. 2006a, MNRAS, 372, 839

Naab, T., Khochfar, S., & Burkert, A. 2006b, ApJ, 636, L81

Ostriker, J. P., & Tremaine, S. D. 1975, ApJ, 202, L113

Patton, D. R., Carlberg, R. G., Marzke, R. O., Pritchet, C. J., da Costa, L. N., & Pellegrini, P. S. 2000, ApJ, 536, 153

Patton, D. R., Pritchet, C. J., Carlberg, R. G., Marzke, R. O., Yee, H. K. C., Hall, P. B., Lin, H., Morris, S. L., Sawicki, M., Shepherd, C. W., & Wirth, G. D. 2002, ApJ, 565, 208

Peng, C. Y., Ho, L. C., Impey, C. D., & Rix, H.-W. 2002, AJ, 124, 266

Pier, J. R., Munn, J. A., Hindsley, R. B., Hennessy, G. S., Kent, S. M., Lupton, R. H., & Ivezić, Ž. 2003, AJ, 125, 1559

Postman, M., & Geller, M. J. 1984, ApJ, 281, 95

Rines, K., Finn, R., & Vikhlinin, A. 2007, ApJ, 665, L9

Scarlata, C., Carollo, C. M., Lilly, S. J., Feldmann, R., Kampczyk, P., Renzini, A., Cimatti, A., Halliday, C., Daddi, E., Sargent, M. T., Koekemoer, A., Scoville, N., Kneib, J.-P., Leauthaud, A., Massey, R., Rhodes, J., Tasca, L., Capak, P., McCracken, H. J., Mobasher, B., Taniguchi, Y., Thompson, D., Ajiki, M., Aussel, H., Murayama, T., Sanders, D. B., Sasaki, S., Shioya, Y., & Takahashi, M. 2007, ApJS, 172, 494

Schlegel, D. J., Finkbeiner, D. P., & Davis, M. 1998, ApJ, 500, 525

Schweizer, F., & Seitzer, P. 1992, AJ, 104, 1039

Smith, G. P., Treu, T., Ellis, R. S., Moran, S. M., & Dressler, A. 2005, ApJ, 620, 78

Smith, J. A., Tucker, D. L., Kent, S., Richmond, M. W., Fukugita, M., Ichikawa, T., Ichikawa, S.-i., Jorgensen, A. M., Uomoto, A., Gunn, J. E., Hamabe, M., Watanabe, M., Tolea, A., Henden, A., Annis, J., Pier, J. R., McKay, T. A., Brinkmann, J., Chen, B., Holtzman, J., Shimasaku, K., & York, D. G. 2002, AJ, 123, 2121

Strateva, I., Ivezić, Ž., Knapp, G. R., Narayanan, V. K., Strauss, M. A., Gunn, J. E., Lupton, R. H., Schlegel, D., Bahcall, N. A., Brinkmann, J., Brunner, R. J., Budavári, T., Csabai, I., Castander, F. J., Doi, M., Fukugita, M., Győry, Z., Hamabe, M., Hennessy, G., Ichikawa, T., Kunszt, P. Z., Lamb, D. Q., McKay, T. A., Okamura, S., Racusin, J., Sekiguchi, M., Schneider, D. P., Shimasaku, K., & York, D. 2001, AJ, 122, 1861

Strauss, M. A., Weinberg, D. H., Lupton, R. H., Narayanan, V. K., Annis, J., Bernardi, M., Blanton, M., Burles, S., Connolly, A. J., Dalcanton, J., Doi, M., Eisenstein, D., Frieman, J. A., Fukugita, M., Gunn, J. E., Ivezić, Ž., Kent, S., Kim, R. S. J., Knapp, G. R., Kron, R. G., Munn, J. A., Newberg, H. J., Nichol, R. C., Okamura, S., Quinn, T. R., Richmond, M. W., Schlegel, D. J., Shimasaku, K., SubbaRao, M., Szalay, A. S., Vanden Berk, D., Vogeley, M. S., Yanny, B., Yasuda, N., York, D. G., & Zehavi, I. 2002, AJ, 124, 1810

Toomre, A. 1977, in Evolution of Galaxies and Stellar Populations, 401–+

Toomre, A., & Toomre, J. 1972, ApJ, 178, 623

Tran, K.-V. H., van Dokkum, P., Franx, M., Illingworth, G. D., Kelson, D. D., & Schreiber, N. M. F. 2005, ApJ, 627, L25

Tucker, D. L., Kent, S., Richmond, M. W., Annis, J., Smith, J. A., Allam, S. S., Rodgers, C. T., Stute, J. L., Adelman-McCarthy, J. K., Brinkmann, J., Doi, M., Finkbeiner, D., Fukugita, M., Goldston, J., Greenway, B., Gunn, J. E., Hendry, J. S., Hogg, D. W., Ichikawa, S.-I., Ivezić, Ž., Knapp, G. R., Lampeitl, H., Lee, B. C., Lin, H., McKay, T. A., Merrelli, A., Munn, J. A., Neilsen, Jr., E. H., Newberg, H. J., Richards, G. T., Schlegel, D. J., Stoughton, C., Uomoto, A., & Yanny, B. 2006, Astronomische Nachrichten, 327, 821

van Dokkum, P. G. 2005, AJ, 130, 2647

van Dokkum, P. G., Franx, M., Fabricant, D., Kelson, D. D., & Illingworth, G. D. 1999, ApJ, 520, L95

Wake, D. A., Nichol, R. C., Eisenstein, D. J., Loveday, J., Edge, A. C., Cannon, R., Smail, I., Schneider, D. P., Scranton, R., Carson, D., Ross, N. P., Brunner, R. J., Colless, M., Couch, W. J., Croom, S. M., Driver, S. P., da Ângela, J., Jester, S., de Propris, R., Drinkwater, M. J., Bland-Hawthorn, J., Pimbblet, K. A., Roseboom, I. G., Shanks, T., Sharp, R. G., & Brinkmann, J. 2006, MNRAS, 372, 537

Weinberg, M. D. 1986, ApJ, 300, 93

Weinmann, S. M., van den Bosch, F. C., Yang, X., & Mo, H. J. 2006, MNRAS, 366, 2

White, M., Zheng, Z., Brown, M. J. I., Dey, A., & Jannuzi, B. T. 2007, ApJ, 655, L69

Yang, X., Mo, H. J., van den Bosch, F. C., & Jing, Y. P. 2005, MNRAS, 356, 1293

York, D. G., Adelman, J., Anderson, J. E., Anderson, S. F., Annis, J., Bahcall, N. A., Bakken, J. A., Barkhouser, R., Bastian, S., Berman, E., & et al. 2000, AJ, 120, 1579

Zehavi, I., Blanton, M. R., Frieman, J. A., Weinberg, D. H., Mo, H. J., Strauss, M. A., Anderson, S. F., Annis, J., Bahcall, N. A., Bernardi, M., Briggs, J. W., Brinkmann, J., Burles, S., Carey, L., Castander, F. J., Connolly, A. J., Csabai, I., Dalcanton, J. J., Dodelson, S., Doi, M., Eisenstein, D., Evans, M. L., Finkbeiner, D. P., Friedman, S., Fukugita, M., Gunn, J. E., Hennessy, G. S., Hindsley, R. B., Ivezić, Ž., Kent, S., Knapp, G. R., Kron, R., Kunszt, P., Lamb, D. Q., Leger, R. F., Long, D. C., Loveday, J., Lupton, R. H., McKay, T., Meiksin, A., Merrelli, A., Munn, J. A., Narayanan, V., Newcomb, M., Nichol, R. C., Owen, R., Peoples, J., Pope, A., Rockosi, C. M., Schlegel, D., Schneider, D. P., Scoccimarro, R., Sheth, R. K., Siegmund, W., Smee, S., Snir, Y., Stebbins, A., Stoughton, C., SubbaRao, M., Szalay, A. S., Szapudi, I., Tegmark, M., Tucker, D. L., Uomoto, A., Vanden Berk, D., Vogeley, M. S., Waddell, P., Yanny, B., & York, D. G. 2002, ApJ, 571, 172

Zibetti, S., White, S. D. M., Schneider, D. P., & Brinkmann, J. 2005, MNRAS, 358, 949

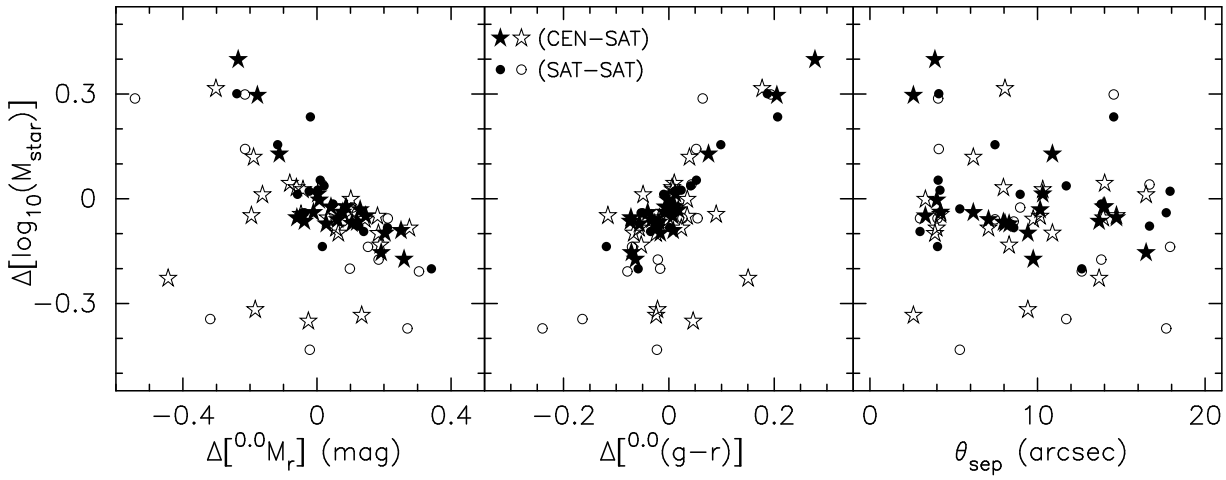

Fig. 13.— The systematic stellar mass uncertainty for progenitors of the 38 massive mergers plotted against the corresponding uncertainty in absolute r-band magnitude, rest-frame $(g-r)$ color, and pair separation. All relative differences between quantities based on SDSS Petrosian and Model magnitudes are such that $\Delta = \mathrm{Petrosian} - \mathrm{Model}$. Solid and open symbols represent galaxy number 1 and 2, respectively.

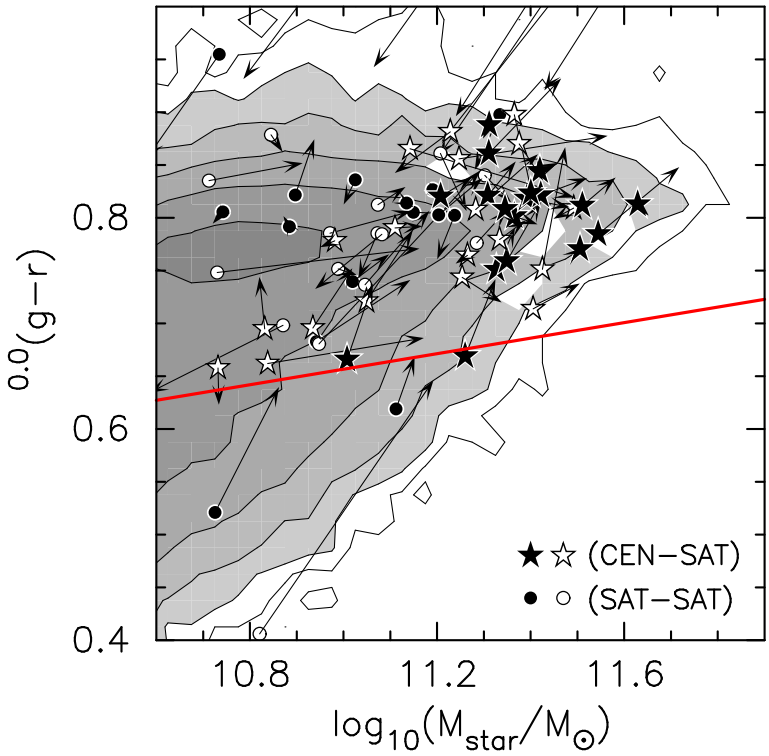

Fig. 14.— Distribution of the 76 massive merger progenitors in color versus stellar mass. Symbols distinguish CEN-SAT (stars) and SAT-SAT (circles) mergers with open symbols representing the progenitor from sampM. Data points are based on Petrosian photometry with arrows showing the offset to ${}^{0.0}(g-r)$ and $\mathrm{M_{star}}$ values using SDSS Model magnitudes (see text for details). The contours and blue/red galaxy division are as in Fig. 2.

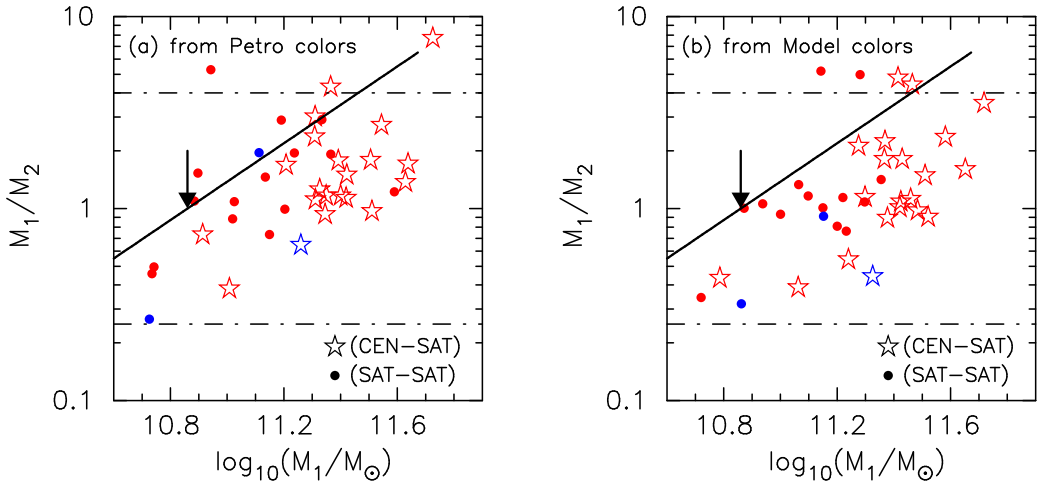

Fig. 15.— Stellar mass ratios of the progenitors of massive major mergers plotted as a function of the stellar mass of progenitor number 1. The two panels show results for color-derived stellar masses based on Petrosian (*left*) and Model (*right*) SDSS magnitudes. Symbols and color coding are as in Fig. 12. The dot-dashed lines show the 4:1 mass ratio boundary of major mergers. Mergers with $\mathrm{M_1/M_2} < 1$ have no redshift for the more-massive primary galaxy (i.e., are spec-phot pairs). Mergers on the solid diagonal line have one progenitor with a mass equal to $\mathrm{M^* = 7.24 \times 10^{10} M_\odot}$ (marked by the arrow).

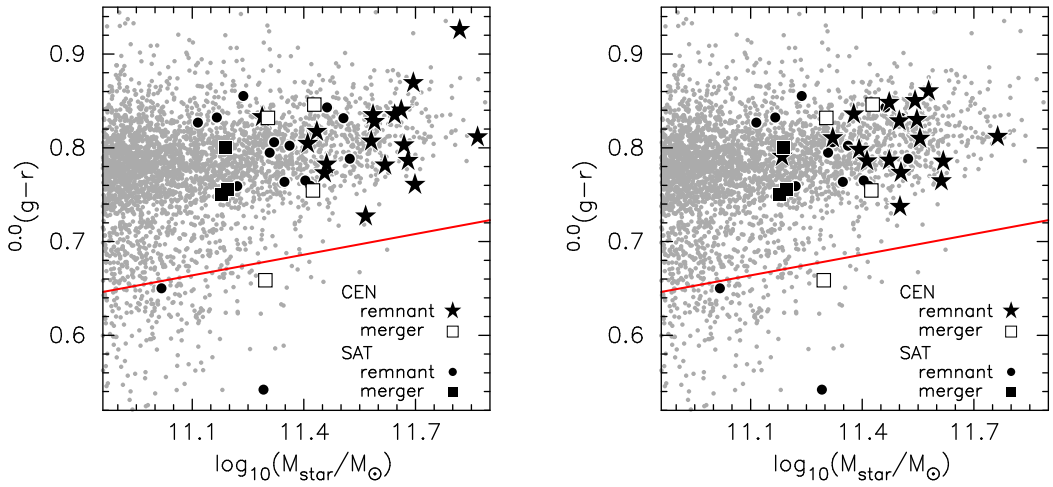

Fig. 16.— Predicted stellar masses and mass-weighted colors of massive merger remnants compared with observations of disturbed-morphology mergers presumed to be nearing final coalescence. Small grey circles show all sampM galaxies more massive than $\mathrm{M^* = 7.24 \times 10^{10} M_\odot}$. Open (CEN) and filled (SAT) squares represent the seven mergers shown in Fig. 3; stars (from CEN-SAT mergers) and circles (from SAT-SAT mergers) represent the predicted remnants of the 38 merger pairs. *Left panel:* the simple assumption that all of the mass from both progenitors is added to the final remnant. *Right panel:* the assumption that 50% of the SAT progenitor mass is added to the ICL if the merger is at the group center. The blue/red galaxy division is as in Fig. 2. All data are based on Petrosian quantities.

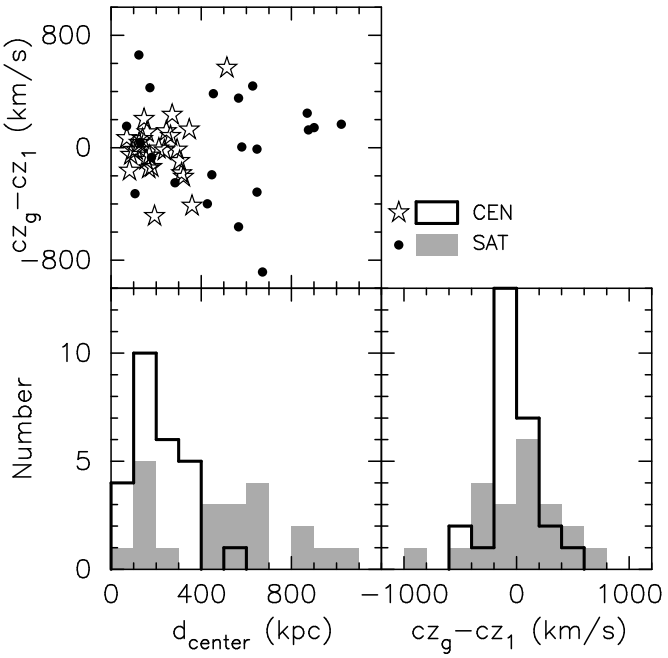

Fig. 17.— Comparison of the group-centric properties of major mergers occurring at group centers (bold lines, stars) or between two SAT galaxies (grey bins, circles). The *top* panel shows the transverse projected offset in kpc versus the radial offset in km/s of each merger relative to the luminosity-weighted group center. The *bottom* panels provide the separate group-centric property distributions.

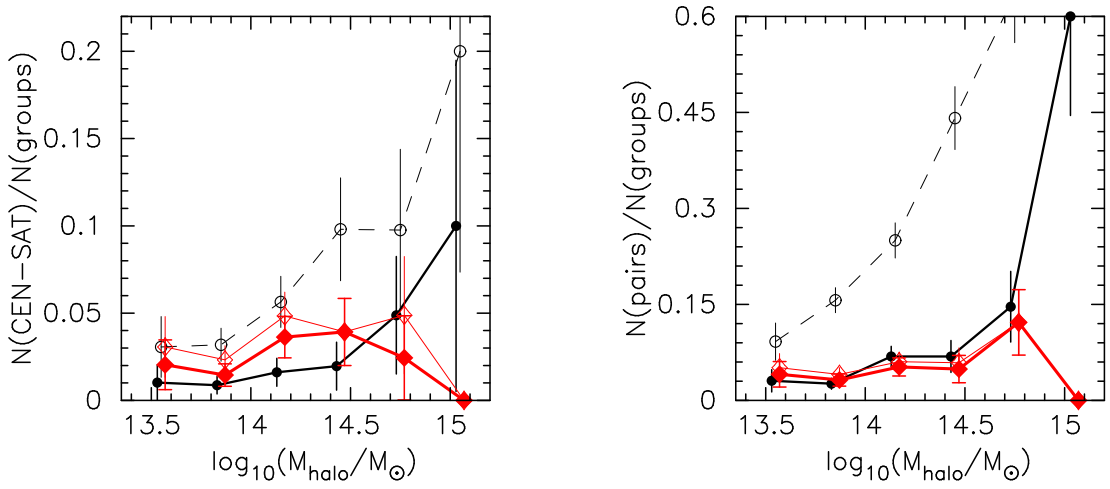

Fig. 18.— Halo-mass dependence for the frequency of major pairs of galaxies with $\mathrm{M_1 + M_2} \geq 10^{11}\mathrm{M_\odot}$ in groups with $\mathrm{M_{halo}} > 2.5 \times 10^{13}\mathrm{M_\odot}$. The fraction of groups with CEN-SAT (left panel) and combined CEN-SAT plus SAT-SAT (right panel) projected pairs are plotted as a function of halo mass in 0.3 dex bins. The dashed line with open circles is for all pairs with $d_{12} \leq 30$ kpc, the solid black line with filled circles is the subset of close pairs that reside in the same host halo (spec-spec only), and the bold red line with filled diamonds denotes the subset of galaxy-galaxy mergers (both spec-spec and spec-phot pairs) identified by our profile fitting method (§2.3). The thin red line with open diamonds in each panel combines the galaxy-galaxy mergers and the additional mergers identified by highly-disturbed morphologies, which provides an upper limit to the number of mergers per group that are detectable in SDSS data. For CEN merging (left panel), this upper limit includes the addition of four SAT-SAT mergers that appear to be at the actual dynamical center of their host halo (see §3.3.1). Poisson errors are shown.

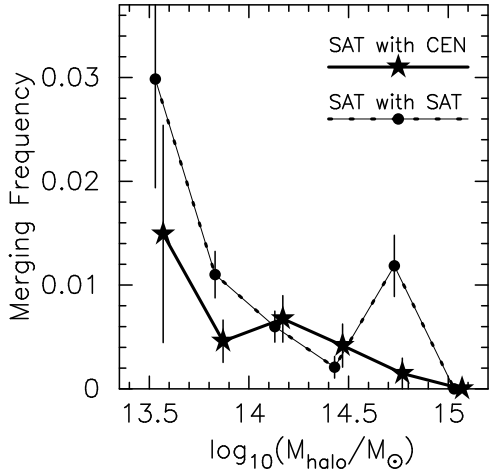

Fig. 19.— Frequency of massive ($\mathrm{M_{star}} \geq 5 \times 10^{10}\mathrm{M_\odot}$) SATs that are involved in merging with either a CEN (solid line with stars) or another massive SAT (dashed line with circles) galaxy, as a function of halo mass. Poisson errors are shown.

Table 1. Massive Galaxy Content in sampM and the $z \leq 0.12$ SDSS DR2 Volume

	stellar-mass bins			
	[10.7,11.0]	[11.0,11.3]	[11.3,11.6]	[11.6,11.9]
Total in DR2 volume	28377	10690	1943	165
Red sequence in DR2 volume	23657	9846	1897	164
Red percent	83.4%	92.1%	97.6%	99.4%
Total in sampM	3238	1415	599	120
Red sequence in sampM	2979	1329	586	119
Red percent	92.0%	93.9%	97.8%	99.2%
Centrals in sampM	29	241	460	115
Percent of DR2 total	0.1%	2.3%	23.7%	69.7%
Satellites in sampM	3209	1174	139	5
Percent of DR2 total	11.3%	11.0%	7.2%	3.0%

Note. — Bins of stellar mass are in units of $\log_{10}(\mathrm{M}_{\odot})$.

Table 2. Progenitors of Massive Merger Systems

Group ID (1)	M_{halo} (2)	Flag (3)	NYU ID (4)	R.A. (5)	Dec (6)	z (7)	M_{star} (8)	$^{0.0}(g-r)$ (9)
121	13.74	CEN	150206	14:14:32.6	+01:43:53.6	0.053	11.21(11.28)	0.82(0.84)
		no	na	14:14:32.6	+01:44:01.5	na	10.98(10.95)	0.78(0.77)
830	13.55	CEN	249473	08:54:58.9	+49:08:32.4	0.052	11.31(11.47)	0.86(0.93)
		no	na	08:55:00.6	+49:08:32.8	na	10.83(10.82)	0.69(0.74)
419	14.41	CEN	9993	12:27:37.1	-00:23:02.4	0.115	11.54(11.72)	0.78(0.85)
		no	na	12:27:36.7	-00:23:10.8	na	11.11(11.17)	0.79(0.79)
54	14.62	CEN	11349	15:08:25.8	-00:15:58.6	0.090	11.63(11.65)	0.81(0.80)
		no	na	15:08:25.0	-00:16:07.1	na	11.49(11.45)	0.81(0.80)
614	13.82	CEN	124158	13:52:02.2	+66:50:20.1	0.068	11.31(11.37)	0.82(0.85)
		no	na	13:52:01.0	+66:50:19.3	na	10.93(11.02)	0.70(0.75)
163	14.47	CEN	175344	15:09:59.4	+03:00:11.1	0.092	11.51(11.58)	0.81(0.84)
		no	na	15:09:59.6	+03:00:03.8	na	11.52(11.21)‡	1.05(0.87)
539	14.30	CEN	222852	00:56:20.1	-09:36:29.7	0.103	11.51(11.51)	0.77(0.77)
		no	na	00:56:20.0	-09:36:33.7	na	11.25(11.34)	0.74(0.72)
393	14.26	CEN	261132	10:04:39.4	+02:57:42.8	0.104	11.37(11.41)	0.80(0.79)
		no	na	10:04:39.5	+02:57:39.9	na	10.73(10.73)	0.66(0.62)
398	14.29	CEN	293645	10:37:29.8	-00:40:40.5	0.096	11.33(11.37)	0.75(0.79)
		no	na	10:37:29.9	-00:40:46.3	na	11.23(11.11)	0.88(0.84)
214	14.18	CEN	311008	15:41:35.7	+55:58:39.8	0.068	11.31(11.30)	0.89(0.87)
		no	na	15:41:34.5	+55:58:38.9	na	11.26(11.24)	0.76(0.76)
291	14.07	CEN	392792	22:28:25.5	-09:37:22.3	0.083	11.35(11.42)	0.76(0.81)
		no	na	22:28:25.6	-09:37:30.4	na	11.28(11.42)	0.81(0.86)
5	14.24	CEN	301558	14:40:42.8	+03:27:55.5	0.027	11.39(11.48)	0.82(0.81)
		SAT	301560	14:40:39.0	+03:28:11.0	0.027	11.14(11.49)‡	0.87(0.82)
102	14.32	CEN	44192	09:58:52.2	+01:03:33.1	0.081	11.26(11.33)	0.67(0.74)
		SAT	44193	09:58:52.0	+01:03:46.4	0.082	11.45(11.68)	1.21(1.06)
759	14.13	CEN	88664	08:46:13.1	+53:26:38.1	0.113	11.73(11.43)‡	1.13(0.92)
		SAT	88665	08:46:13.3	+53:26:35.9	0.113	10.84(11.17)‡	0.66(0.69)
74	14.27	CEN	258681	11:45:37.2	+64:30:41.4	0.063	11.42(11.46)	0.84(0.85)
		SAT	258682	11:45:37.4	+64:30:45.3	0.064	11.37(11.41)	0.90(0.81)
847	13.91	CEN	274752	10:34:09.7	+04:21:29.8	0.100	11.42(11.52)	0.82(0.84)
		SAT	274751	10:34:09.1	+04:21:30.8	0.100	11.25(11.56)‡	0.86(0.88)
572	13.92	CEN	371303	13:30:10.3	-02:06:18.0	0.087	11.35(11.38)	0.81(0.79)
		SAT	371304	13:30:10.9	-02:06:13.6	0.086	11.38(11.43)	0.87(0.84)
1775	13.98	CEN	92509	17:20:36.1	+56:39:42.5	0.120	11.40(11.42)	0.82(0.83)
		SAT	92510	17:20:37.7	+56:39:45.1	0.120	11.33(11.39)	0.78(0.80)
1545	13.43	SAT	364190	13:36:43.6	-03:29:57.0	0.053	10.91(10.79)	1.01(0.93)

Table 2—Continued

Group ID (1)	M_{halo} (2)	Flag (3)	NYU ID (4)	R.A. (5)	Dec (6)	z (7)	M_{star} (8)	$^{0.0}(g-r)$ (9)
		no†	na	13:36:44.3	-03:29:52.5	na	11.05(11.15)	0.72(0.79)
126	13.55	SAT	367419	13:59:25.2	-03:12:29.0	0.025	10.73(10.58)	0.95(0.86)
		no	na	13:59:24.8	-03:12:33.1	na	11.07(11.13)	0.81(0.83)
37	14.72	SAT††	33684	15:11:20.3	-00:07:20.1	0.089	11.02(11.10)	0.74(0.77)
		no††	na	15:11:19.2	-00:07:16.5	na	11.07(11.03)	0.79(0.74)
72	14.79	SAT	83539	08:54:48.7	+00:51:02.6	0.107	11.11(11.15)	0.62(0.67)
		no	na	08:54:48.2	+00:50:46.6	na	10.82(11.19)‡	0.41(0.65)
2955	13.81	SAT	206506	20:45:09.4	-06:17:05.5	0.112	10.88(10.87)	0.79(0.80)
		no	na	20:45:08.9	-06:17:01.5	na	10.85(10.87)	0.88(0.86)
81	14.37	SAT	218908	23:37:05.4	+15:55:58.5	0.066	10.94(11.14)	0.68(0.74)
		no	na	23:37:06.2	+15:56:03.2	na	10.22(10.43)	0.49(0.57)
219	14.20	SAT††	223211	23:54:59.6	-09:14:49.4	0.074	11.03(11.00)	0.84(0.81)
		no††	na	23:54:59.7	-09:14:53.0	na	10.99(11.03)	0.75(0.75)
14	14.83	SAT	278870	10:39:39.0	+05:10:31.3	0.068	10.73(10.86)	0.52(0.64)
		no	na	10:39:38.7	+05:10:32.6	na	11.30(11.36)	0.84(0.81)
1786	13.99	SAT	284077	14:31:09.6	+60:41:18.4	0.113	10.74(10.72)	0.81(0.79)
		no	na	14:31:10.2	+60:41:35.7	na	11.05(11.18)	0.74(0.81)
344	13.92	SAT	333778	12:40:30.2	+05:52:21.5	0.075	11.59(11.36)	1.36(1.15)
		no	na	12:40:30.9	+05:52:10.6	na	11.50(11.20)‡	1.05(0.86)
261	14.26	SAT	336039	17:01:52.2	+35:02:54.9	0.107	11.01(11.06)	0.67(0.74)
		no†	na	17:01:53.1	+35:03:04.0	na	11.43(11.47)	0.75(0.87)
75	14.85	SAT	346478	12:47:56.7	+62:36:27.6	0.107	11.33(11.28)	0.90(0.85)
		no	na	12:47:56.7	+62:36:23.5	na	10.87(10.58)	0.70(0.63)
170	13.88	SAT††	352171	13:33:03.2	+60:07:00.0	0.072	11.37(11.06)‡	1.13(0.94)
		no††	na	13:33:03.4	+60:07:03.7	na	11.08(10.94)	0.78(0.73)
479	14.28	SAT	373137	14:09:59.4	-01:32:18.9	0.117	11.64(11.24)‡	1.17(0.90)
		no†	na	14:09:59.5	-01:32:22.8	na	11.41(11.51)	0.71(0.74)
1047	13.97	SAT	393494	22:22:48.8	-09:02:14.4	0.084	11.15(11.23)	0.81(0.80)
		no	na	22:22:49.0	-09:02:22.2	na	11.28(11.35)	0.78(0.81)
462	13.91	SAT	250588	08:36:45.9	+47:22:10.2	0.053	11.13(11.15)	0.81(0.81)
		SAT	250589	08:36:44.8	+47:22:18.9	0.053	10.97(11.15)	0.79(0.81)
714	13.60	SAT	604118	15:28:12.7	+42:55:47.7	0.019	10.90(10.94)	0.82(0.87)
		SAT	604117	15:28:16.7	+42:56:38.8	0.018	10.71(10.91)	0.84(0.85)
460	14.24	SAT	241625	09:55:39.5	+01:35:48.4	0.099	11.24(11.20)	0.80(0.76)
		SAT	241629	09:55:40.2	+01:35:50.3	0.099	10.95(11.29)‡	0.68(0.84)
465	14.13	SAT††	294450	10:50:25.4	-00:20:11.1	0.096	11.20(11.30)	0.80(0.84)
		SAT††	294451	10:50:25.5	-00:20:10.1	0.093	11.21(11.26)	0.86(0.81)

Table 2—Continued

Group ID (1)	$\mathrm{M_{halo}}$ (2)	Flag (3)	NYU ID (4)	R.A. (5)	Dec (6)	z (7)	$\mathrm{M_{star}}$ (8)	$^{0.0}(g-r)$ (9)
337	14.12	SAT	269340	09:22:22.2	+02:35:09.3	0.088	$11.19(11.22)$	$0.83(0.82)$
		SAT	269341	09:22:22.0	+02:35:13.8	0.087	$10.73(11.16)^{\ddagger}$	$0.75(0.77)$

Note. — For each merger pair the progenitor properties are listed on two separate lines with the following columns: group ID number (1) and dark-matter halo mass estimate in units of $\log_{10}(\mathrm{M}_{\odot})$ (2) from the public SDSS DR2 group catalog of Yang et al.; flag (3) for whether galaxy was identified in group catalog as a central (CEN), satellite (SAT), or not identified (no) owing to no spectroscopic redshift; ID number (4), epoch J2000.0 celestial coordinates (5,6), and spectroscopic redshift (7) from the NYU-VAGC; stellar mass estimates in units of $\log_{10}(\mathrm{M}_{\odot})$ (8) based on SDSS Petrosian(Model) photometry and Bell et al. (2003) M/L ratios; rest-frame K-corrected to $z = 0.0$ color (9) from SDSS Petrosian(Model) photometry.

† Estimated stellar mass of the companion exceeds that of the spectroscopic CEN galaxy of the host; the merger is added to the CEN-SAT subset in the analysis.

†† Total estimated stellar mass of the two SATs ($\mathrm{M}_1 + \mathrm{M}_2$) exceeds that of the spectroscopic CEN galaxy of the host; including/excluding the merger to the CEN-SAT subset is analyzed.

‡ More than factor of 2 difference (0.3 dex) between Petrosian and Model-based $\mathrm{M_{star}}$ estimates.